Copernicus Sentinel-3 Surface Topography Mission - Cyclic Performance Report

MWR

S3A	S3B
Cycle No. 98 Start date: 17/04/2023 End date: 14/05/2023	Cycle No. 79 Start date: 27/04/2023 End date: 24/05/2023

Reference: S3MPC-STM_CPR_0006_097_078

Issue 1.1 – 03/06/2023

Contract: 4000136824/21/I-BG

Open/Public/Público

CHRONOLOGY ISSUES

Issue	Date	Object	Written by	Checked by	Approved by
1.0	07/01/2022	Creation	M. Denneulin	J. Aublanc	G. Jettou
1.1	09/08/2022	Monitoring over Caspian Sea	M. Denneulin	J. Aublanc	G. Jettou

ACCEPTANCE

	CLIENT: ESA	SUPPLIER: CLS
Name	Pierre Féménias	Ghita Jettou
Function	ESA Technical Officer	MPC Service Manager

LIST OF CONTENTS

LIST OF TABLES

LIST OF FIGURES

1 Introduction

The purpose of this document is to report on the performance and data quality of the Copernicus Sentinel-3 Surface Topography Mission (STM) LAND products. The constellation currently includes Sentinel-3A and Sentinel-3B altimetry satellites. This document is associated with data dissemination on a cyclic basis and is generated a few days after the end of Sentinel-3B cycle.

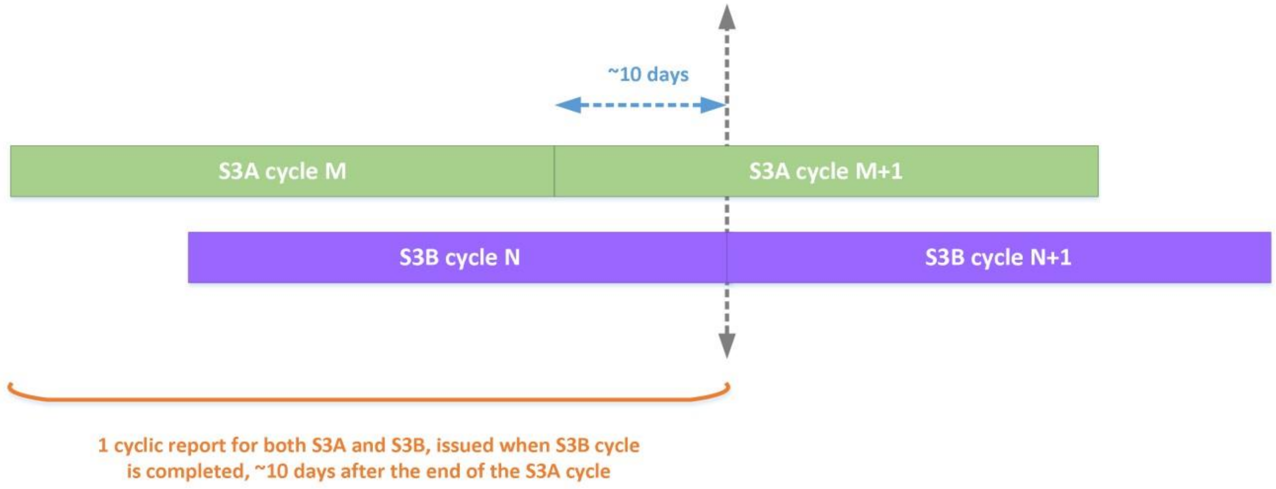

Figure 1: S3A and S3B cycles chronology

The MWR Level 1 products and SRAL/MWR Level 2 products assessed hereafter are produced by the ESA Sentinel-3 LAND Processing Centre. One of the main goals of the cyclic report is to detect and report as quickly as possible any events, or anomaly, impacting the data quality. Subsequently, the assessments are made on the Short Time Critical (STC) products, generally delivered 48 hours after data acquisitions. Differences are expected with the Non Time Critical (NTC) products, for which the orbit data and several geophysical corrections are consolidated.

The main objectives of this document are:

- To provide a data quality assessment of the Sentinel-3 MWR Level 1 STC LAND products
- To provide a data quality assessment of the Sentinel-3 MWR/SRAL Level 2 STC LAND products
- To report on any changes likely to impact data quality at any level, from instrument status to software configuration.
- To present the major useful results for S3A cycle 98, from 17/04/2023 to 14/05/2023.
- To present the major useful results for S3B cycle 79, from 27/04/2023 to 24/05/2023.

2 Cycle overview

The Table 1 gives a summary of the instrument behavior for S3A and S3B respectively during this period.

	Analysis	Status	Comments
S3A	Instrument	🟢	Nominal
	Internal Calibration	🟢	Nominal
	Geophysical products	🟢	Nominal
	Long-term monitoring	🟢	Nominal
S3B	Instrument	🟢	Nominal
	Internal Calibration	🟢	Nominal
	Geophysical products	🟢	Nominal
	Long-term monitoring	🟢	Nominal

Table 1 : General overview of the S3A MWR quality assessment

Color legend:

🟢	OK	🔴	NOK
🟠	Warning	⚪	Not available

3 Processing baseline

Table 2 details the versions of the Processing Baseline (PB), and Level-1 and Level-2 Instrument Processing Facility software used for the products assessed. This is part of the Baseline Collection (BC) 004.

	Cycle	Processing Baseline	IPF SM2 version	IPF SR1 version	IPF MW1 version
Sentinel-3A Sentinel-3B	98 79	3.05	06.20	06.20	06.13

Table 2: Processing baseline and IPF details

The evolutions of the Sentinel-3 STM Processing Baseline since July 2016, end of commissioning phase, are summarized in the "Sentinel Online" Web pages: https://sentinels.copernicus.eu/web/sentinel/technical-guides/sentinel-3-altimetry/processing-baseline

4 MWR Monitoring

This section is dedicated to the functional verification of the MWR sensor behaviour. The main relevant parameters, monitored daily by the MPC team, are presented here.

4.1 Operating modes

The radiometers on-board S3A and S3B have several operating modes listed hereafter:

- Mode 0 : Intermonitoring (Earth observation)
- Mode 1 : Monitoring
- Mode 2 : Noise Injection calibration
- Mode 3 : Dicke Non-Balanced calibration (100% injection – hot point)
- Mode 4 : Dicke Non-Balanced calibration (50% injection – cold point)

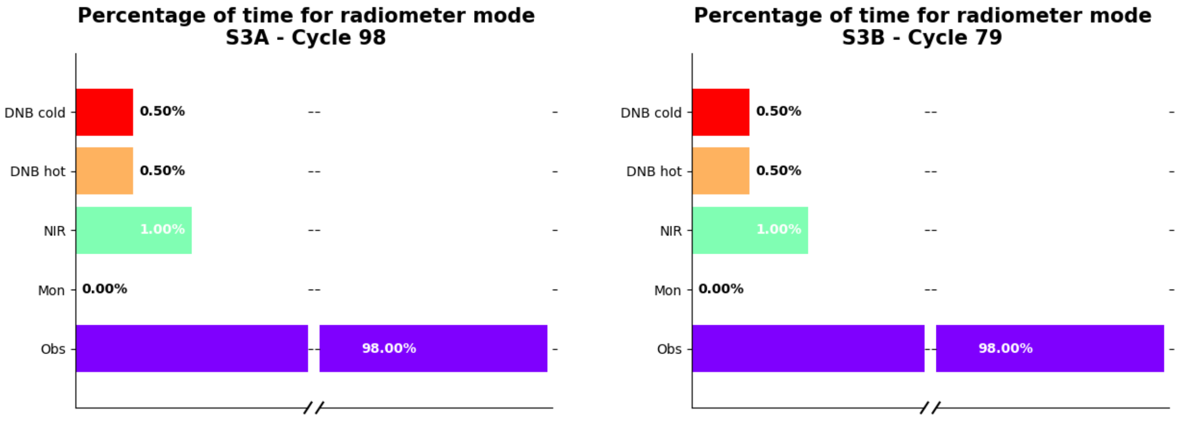

Figure 2 : Distribution of operating mode (S3A: left; S3B: right)

The distribution has slightly changed with respect to the beginning of the mission due to update of calibration timeline of the 1st March 2018. Before the update, a calibration sequence is 9s long composed of and occurs 3 times per orbit. After that update, the calibration sequences are much shorter (~0.6s) but occurs every 30 seconds. Moreover, due to more frequent calibration, the monitoring measurements are no longer needed to monitore the noise diode.

Concerning measurements in the Intermonitoring mode (Obs mode), two kind of processing can be used according to the measured brightness temperature. If this temperature is smaller than the reference load inside the instrument, the NIR processing is used; if the temperature is greater, the DNB processing is used. The transition from one processing to the other will occur more or less close to the coast depending on the internal temperature of the MWR. The internal temperature of the MWR is such that only a small percentage of measurements required a DNB processing in this cycle as shown by Figure 2 for S3A and S3B.

This figure shows also the passage over the US KREMS radar facility in the Kwajalein atoll (9°23'47'' N - 167°28'50'' E) in the Pacific. For safety reasons, the MWR is switched to a specific mode about 50 km before the facility location and back to nominal mode 50km after. From the 17th January, the safing area was enlarged to 300km during the investigations. It was reduced to ~100km the 29th May 2019.

Note: A lunar calibration of the OLCI instruments on 06/05/2023 that started at 04:52 and ended at 05:44 degraded STC production resulting in Brightness temperature data gaps. Figure 3 shows a blue arc that corresponds to brightness temperatures at default values in addition to the US KREMS location.

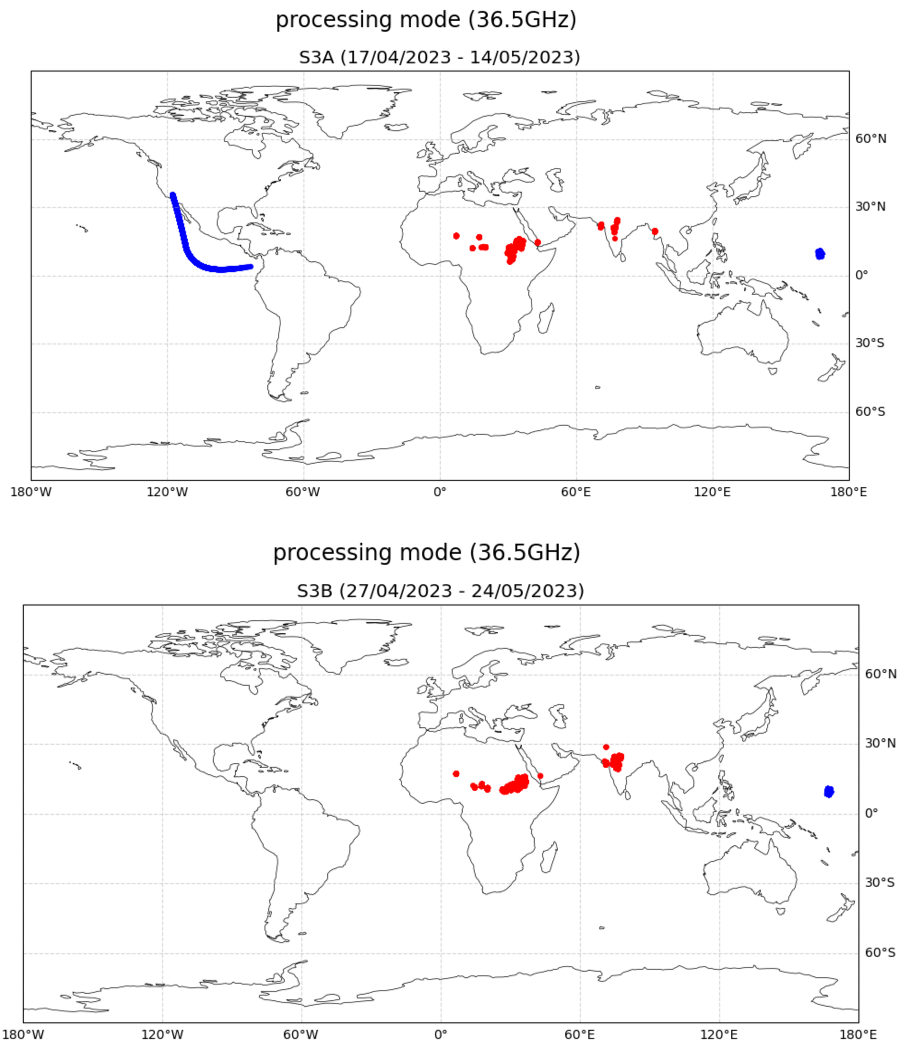

Figure 3 : Map of measurements with DNB processing for 36.5GHz channel (red) and safety mode for both channels over KREMS (blue dot) (S3A on top panel, S3B bottom panel)

4.2 Calibration parameters

To monitor the instrument behaviour during its lifetime, the relevant parameters of the MWR internal in-flight calibration procedure are presented in the following subsections. These parameters are:

- the gain: this parameter is estimated using the two types of Dicke Non-Balanced calibration measurements (100% and 50% of injection). The DNB processing of the Earth measurements uses this parameter.
- the noise injection temperature: this parameter is measured during the Noise Injection calibration measurements. The NIR processing of the Earth measurements uses this parameter.

4.2.1 Gain

4.2.1.1 Sentinel-3A

Figure 4 shows the monitoring of the receiver gain over one cycle of S3A. The mean value over the cycle is 4.82mv/K and 4.6mV/K for channel 23.8GHz and 36.5GHz respectively. These values are close to values estimated on-ground during characterization of the instrument (4.83mV/K and 4.59mV/K for channels 23.8GHz and 36.5GHz respectively).

For both channels, nominal behavior is observed since only 1 cycle of data is considered in this section.

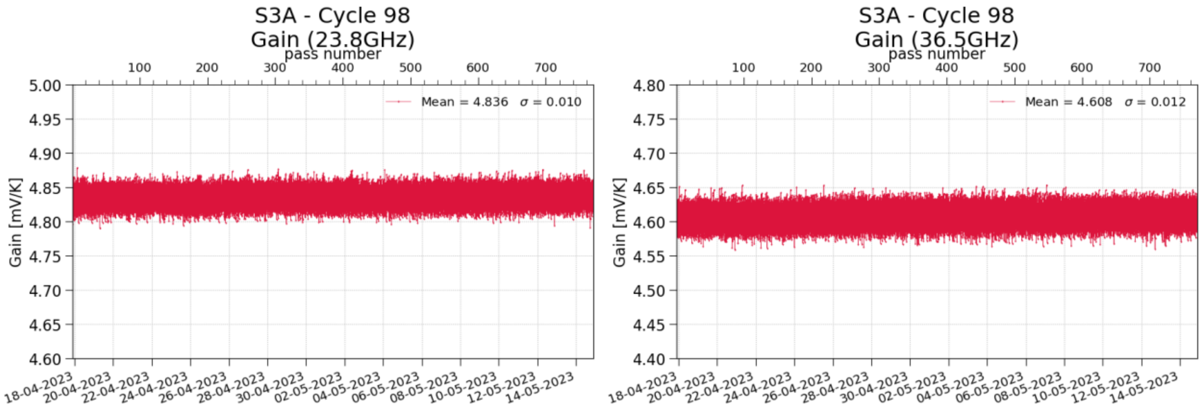

Figure 4 : S3A Monitoring of receiver gain for both channels :23.8GHz (left) and 36.5GHz (right)

4.2.1.2 Sentinel-3B

Figure 5 shows the monitoring of the receiver gain over one cycle of S3B. The mean value over the cycle is 4.54mv/K and 4.45mV/K for channel 23.8GHz and 36.5GHz respectively. These values are close to values estimated on-ground during characterization of the instrument (4.54mV/K and 4.46mV/K for channels 23.8GHz and 36.5GHz respectively).

For both channels, nominal behavior is observed since only 1 cycle of data is considered in this section.

Note: A small jump in the values of the gain for the 36.5GHz channel can be observed, the reason for this behaviour is still under investigation, but this should not affect radiometer performances.

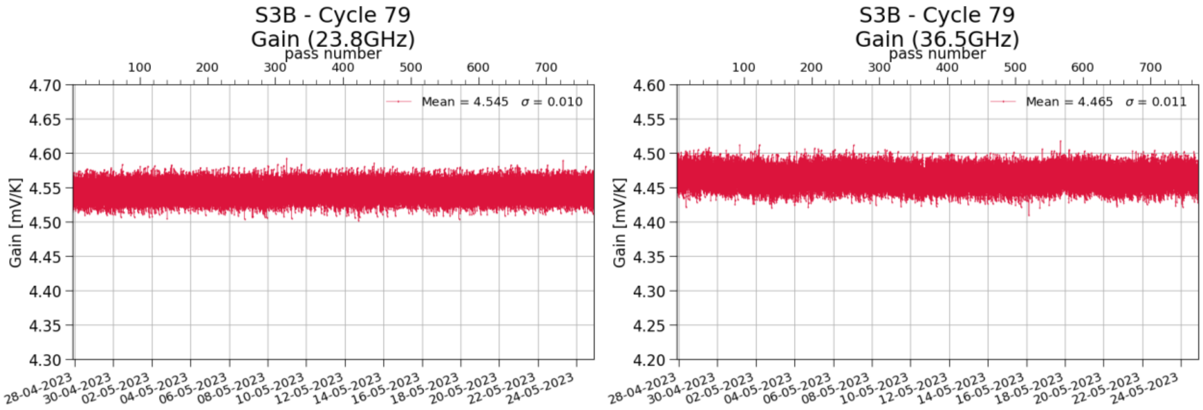

Figure 5 : S3B Monitoring of receiver gain for both channels :23.8GHz (left) and 36.5GHz (right)

4.2.2 Noise Injection Temperature

4.2.2.1 Sentinel-3A

Figure 6 shows the monitoring of the noise injection temperature over one cycle of S3A. The noise injection temperatures show no trend over the cycle for both channels. The average value of the noise injection temperatures are 312.9K/289.1K for channels 23.8GHz/36.5GHz respectively.

For both channels, nominal behavior is observed since only 1 cycle of data is considered in this section.

Figure 6 : Monitoring of S3A Noise Injection temperature for both channels :23.8GHz (left) and 36.5GHz (right)

4.2.2.2 Sentinel-3B

Figure 7 shows the monitoring of the noise injection over one cycle of S3B. The noise injection temperature shows no trend over the cycle for both channels. The average value of the noise injection tempeartures are 311.5K/311.5K for channels 23.8GHz/36.5GHz respectively.

For both channels, nominal behavior is observed since only 1 cycle of data is considered in this section.

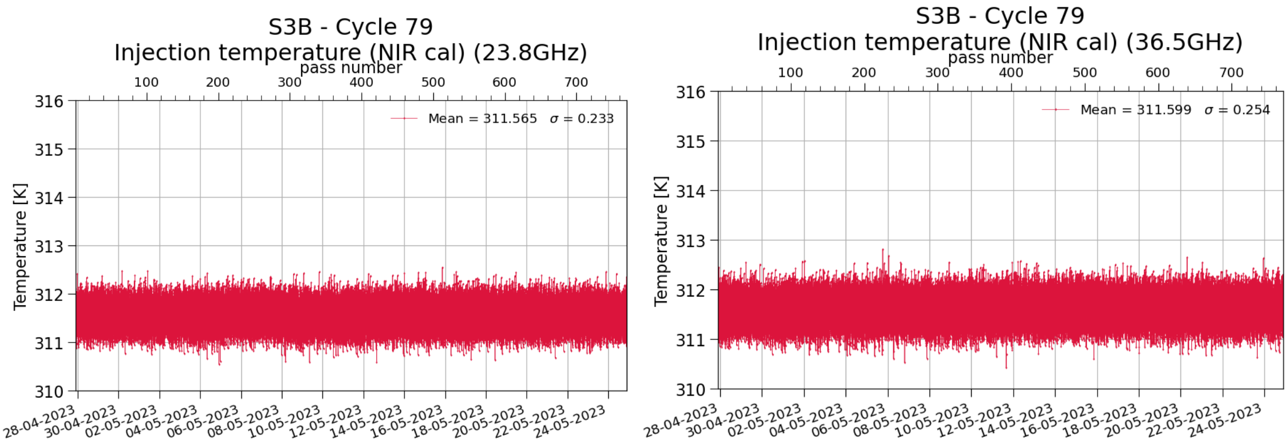

Figure 7 : Monitoring of S3B Noise Injection temperature for both channels :23.8GHz (left) and 36.5GHz (right)

4.3 Brightness Temperatures

The two following figures show maps of brightness temperatures for the two channels of S3A split by ascending (right part) and descending (left part) passes. Figure 8 and Figure 9 concern the channels 23.8GHz and 36.5GHz respectively. These maps show a good contrast between ocean and land for both channels.

Note: due to a special operation for the OLCI instrument on the 6th of May 2023, data of an ascending pass of S3A are degarded.

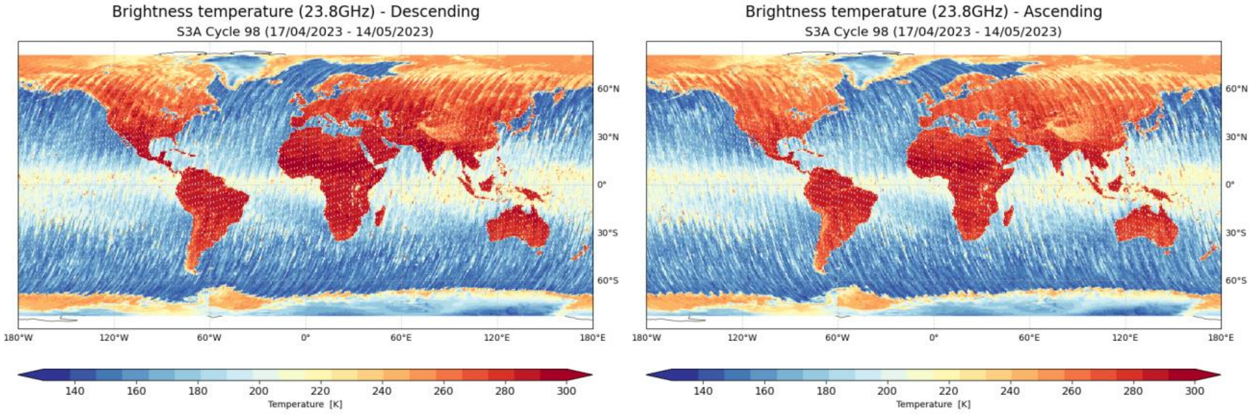
Brightness temperature (23.8GHz) - Descending
S3A Cycle 98 (17/04/2023 - 14/05/2023)

Brightness temperature (23.8GHz) - Ascending
S3A Cycle 98 (17/04/2023 - 14/05/2023)

Figure 8 : Map of S3A Brightness temperatures of channel 23.8GHz for ascending (right) and descending (left) passes

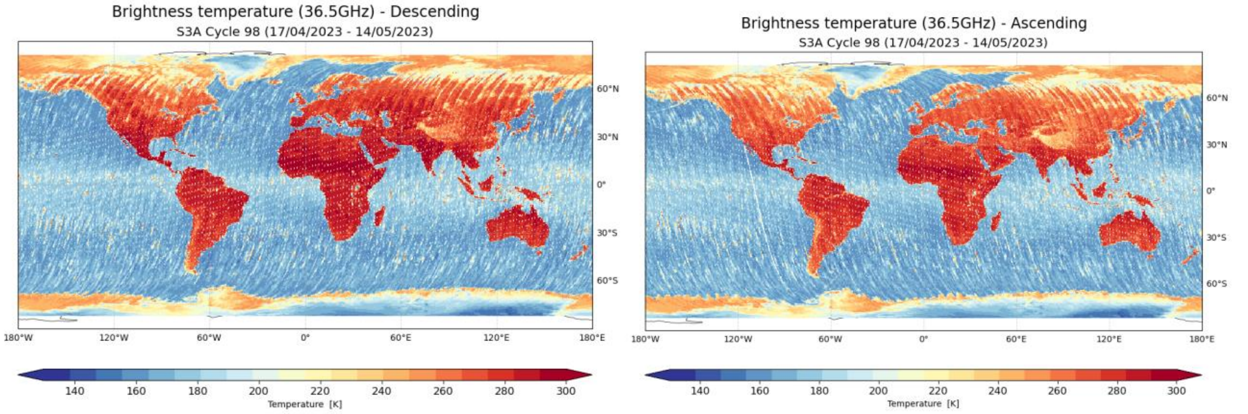
Brightness temperature (36.5GHz) - Descending
S3A Cycle 98 (17/04/2023 - 14/05/2023)

Brightness temperature (36.5GHz) - Ascending
S3A Cycle 98 (17/04/2023 - 14/05/2023)

Figure 9 : Map of S3A Brightness temperatures of 36.5GHz channel for ascending (right) and descending (left) passes

Figure 10 and Figure 11 concern the channels 23.8GHz and 36.5GHz respectively also split by ascending (right part) and descending (left part) passes. These maps show a good contrast between ocean and land for both channels.

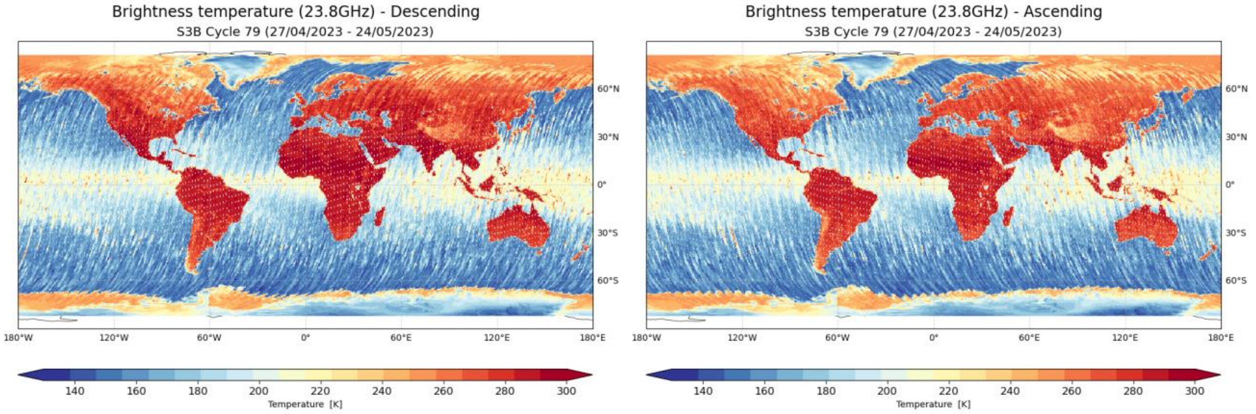
Brightness temperature (23.8GHz) - Descending
S3B Cycle 79 (27/04/2023 - 24/05/2023)

Brightness temperature (23.8GHz) - Ascending
S3B Cycle 79 (27/04/2023 - 24/05/2023)

Figure 10 : Map of S3B Brightness temperatures of channel 23.8GHz for ascending (right) and descending (left) passes

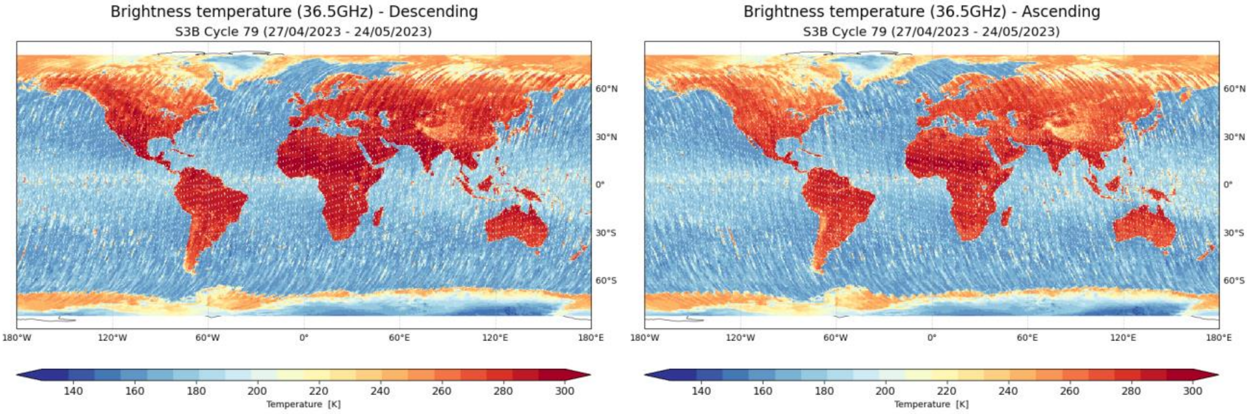

Figure 11 : Map of S3B Brightness temperatures of channel 36.5GHz for ascending (right) and descending (left) passes

From these pictures, we can see that S3A and S3B brightness temperatures seem to be close, but they do not provide an accurate number. Figure 12 shows histograms of MWR brightness temperatures over ocean for S3A and S3B for the period corresponding to the Cycle 98 of S3A. We can see how close the two instruments are after the intercalibration. It subsists a bias of only 0.6K for 23.8GHz and 0.1K for 36.5GHz as expected from the commissioning results.

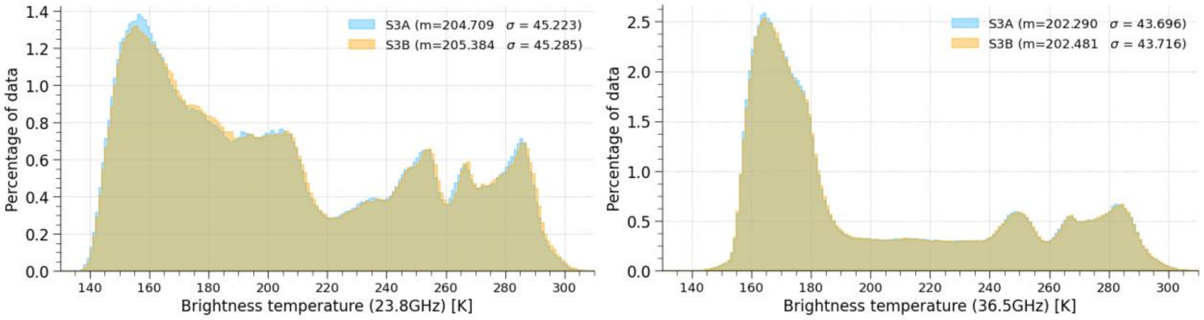

Figure 12 : Histogram of S3A and S3B brightness temperatures (all surfaces) for 23.8GHz (left) and 36.5GHz (right) channels

5 Long-term monitoring

In this section, a long-term monitoring of the MWR behaviour is presented.

5.1 Internal Calibration parameters

5.1.1 Gain

5.1.1.1 Sentinel-3A

Figure 13 shows the daily mean of the receiver gain for both channels. This calibration parameter is used in the DNB processing of the measurements. As seen previously in section 4.1, only a small part of the measurements are processed in DNB mode. The first part of the monitoring of the calibration parameters shown here is performed with products generated during the reprocessing using the processing baseline 2.15, the second part using NRT products from the day of the IPF update on the Svalbard ground station forward.

From the two panels of Figure 13, one can see that the receiver gain has a different evolution for each channel. The gain for the 23.8GHz channel has slowly increased since the beginning of the mission showing four slopes and three inflexion points at August 2016, Februray 2017 and June 2017. It seems to be almost stable since cycle 19 (July 2017). The gain has increased of +0.07mv/K since the beginning of the mission. The update of the calibration timeline of the 1st March 2018 has an impact on the standard deviation and minimum and maximum values of the gain for both channels (as explained in section 4.2.1), but there is no evidence of a change in the daily mean value.

The gain of the 36.5GHz channel is showing a slow decrease with a seasonal oscillation. The RFI with KREMS radar facility of November 2018 (cycle 38) changes the operating point of the radiometer and the level of the gain. After a period of stabilisation, the gain retrieved its slow decrease. In February 2019, an update of the ground processing software is responsible for the small jump visible for both channels.

Spurious values in the statistics are observed at several occasions due to a special operation for the OLCI instrument: 4th July 2020 (cycle 60), 18th January 2022 (cycle 81), 13th July (cycle 87), 10th September (cycle89) , 11th November (cycle 92), 7th January (cycle 94), 7th March (cycle96) and 6th of May (Cycle 98).

Due to the small number of data processed using this parameter, it will be difficult to assess if this decrease has an impact on data quality. The monitoring will be pursued and data checked for any impact.

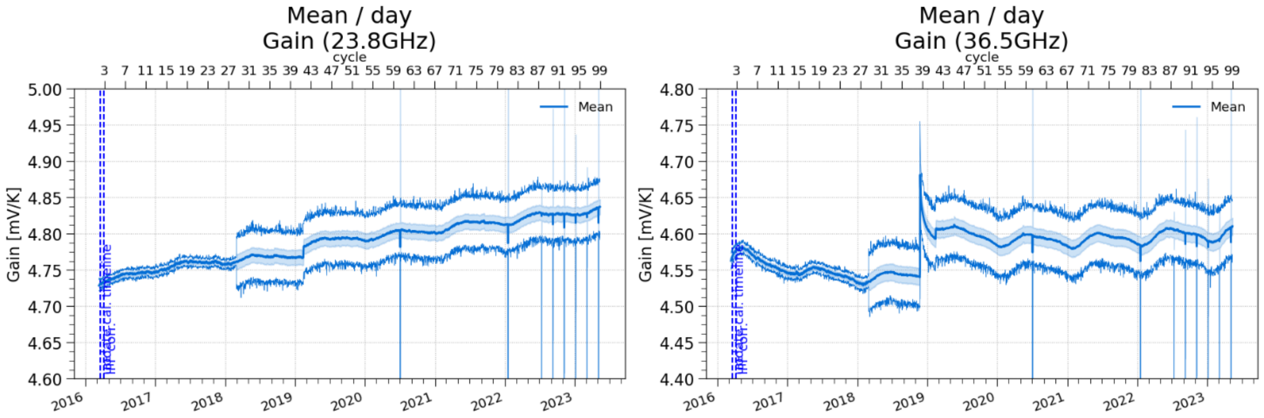

Figure 13 : Daily mean of the gain for both channels : 23.8GHz (left) and 36.5GHz (right)

5.1.1.2 Sentinel-3B

Figure 14 shows the daily mean of the receiver gain for both channels of Sentinel-3B. The monitoring of the calibration parameters shown here is performed with products generated operationaly by the Land Processing center (LN3).

From the two panels of Figure 14, one can see that the receiver gain has a different evolution for each channel. The gain for the 23.8GHz channel has slowly increased since the beginning of the mission and seems stabilized since September 2018. The update of the MWR characterization file of the 6th December 2018 caused the change of value in the computed value of the gain observable at that date. The gain of the 36.5GHz channel decreasd during the first months of the mission and seems stabilized since September 2018. A small step at the beginning of December is also observable, with the same cause than for the 23.8GHz channel (update of the characterization file).

In February 2019, an update of the ground processing software is responsible for the small jump visible for both channels.

Spurious values in the statistics are observed at several occasions due to a special operation for the OLCI instrument: 16th February 2022 (cycle 62), 11th August (cycle 69), 10th October (cycle71), 08th December (cycle 73) and 6th Februrary 2023 (cycle 76) and 6th April 2023 (cycle 78)

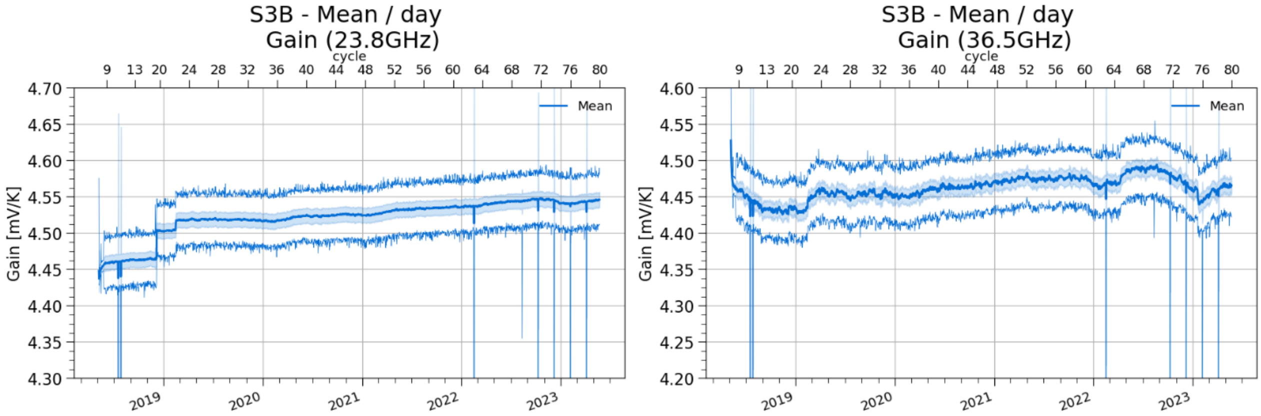

Figure 14 : Daily mean of the gain for both channels : 23.8GHz (left) and 36.5GHz (right)

5.1.2 Noise Injection temperature

5.1.2.1 Sentinel-3A

Figure 15 shows the daily mean of the noise injection temperature for both channels of Sentinel-3A. This calibration parameter is used in the NIR processing of the measurements. As seen previously in section 4.1, the main part of the measurements are processed in NIR mode. Moreover the first part of the monitoring of the calibration parameters is performed using products generated during the reprocessing of processing baseline 2.15, the second part using NRT calibration products from the day of the IPF update on the ground station.

From the two panels of Figure 15, one can see that the noise injection parameter has a different evolution for each channel. The noise injection temperature of 23.8GHz channel has decreased of less than 0.5K during the first 2 cycles, after what there has been no significant change of behaviour until cycle 13. During this cycle, the noise injection temperature seems to start a slow decrease. The injection temperature of the 36.5GHz channel is not stable : it seems to follow some kind of seasonal signal combined with a trend. The monitoring will be pursued and data checked for any impact.

The update of the calibration timeline of the 1st March 2018 has an impact on the standard deviation and minimum and maximum values of the gain (as explained in section 4.2.1), but there is no evidence of a change in the daily mean value.

Some peak values are noticeable at the end of cycle 4 (mainly channel 23.8GHz), at the end of cycle 6, during cycle 9, 10, 12 and 16. Some of these peaks concerns both channels at the same time, while a small part of them only one of them. The investigations performed in the cycle 6 report has shown that these measurements are localized around a band of latitude that may change along the time series. The source is not yet clearly identified but a intrusion of the Moon in the sky horn is suspected.

A step of ~0.2K is seen during cycle 38 as observed in section 4.2.2. Investigations carried out have shown that a RFI around the KREMMS facility caused a stress to the MWR.

A step of ~0.1K for injection temperature at 23.8GHz channel is seen during cycle 76 (pass 501). The step is so small that it can be seen only on statistics per day or per pass (not on cycle timeseries as presented in section 4.2.2.1).

Spurious values in the statistics are observed at several occasions due to a special operation for the OLCI instrument: 4th July 2020 (cycle 60), 18th January 2022 (cycle 81), 13th July (cycle 87), 10th September (cycle89) , 11th November (cycle 92), 7th January (cycle 94), 7th March (cycle96) and 6th of May (Cycle 98).

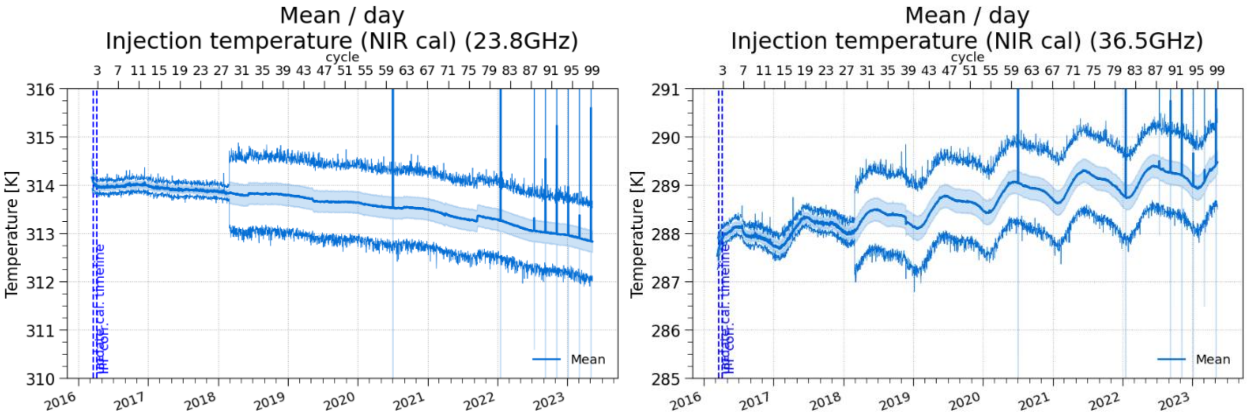

Figure 15 : Sentinel3-A Daily statistics of the noise injection temperature for channel 23.8GHz (left) and 36.5GHz (right): mean (bold line), min/max (thin line), standard deviation (shade)

5.1.2.2 Sentinel-3B

Figure 16 shows the daily mean of the noise injection temperature for both channels of Sentinel-3B. This calibration parameter is used in the NIR processing of the measurements. The monitoring of the calibration parameters shown here is performed with products generated operationaly by the Land Processing center (LN3).

From the two panels of Figure 16, one can see that the noise injection parameter has a different evolution for each channel. The noise injection temperature of the 23.8GHz channel has increased at the beginning of the mission and seems stabilized since September. The injection temperature of the 36.5GHz channel is not stable : it seems to follow a trend. The two peaks observed in July 2018 are due to a maneuver for cold sky seeing (17 July 2018) in preparation for Moon seeing maneuver (27 July 2018).

A step occurs in April 2019 and is observable only for this parameter (not the gain) and only for the 23.8GHz channel. Investigations showed that no RFI or known event are responsible for this change of behavior.

Spurious values in the statistics are observed at several occasions due to a special operation for the OLCI instrument: 16th February 2022 (cycle 62), 11th August (cycle 69), 10th October (cycle71), 08th December (cycle 73) and 6th Februrary 2023 (cycle 76) and 6th April 2023 (cycle 78)

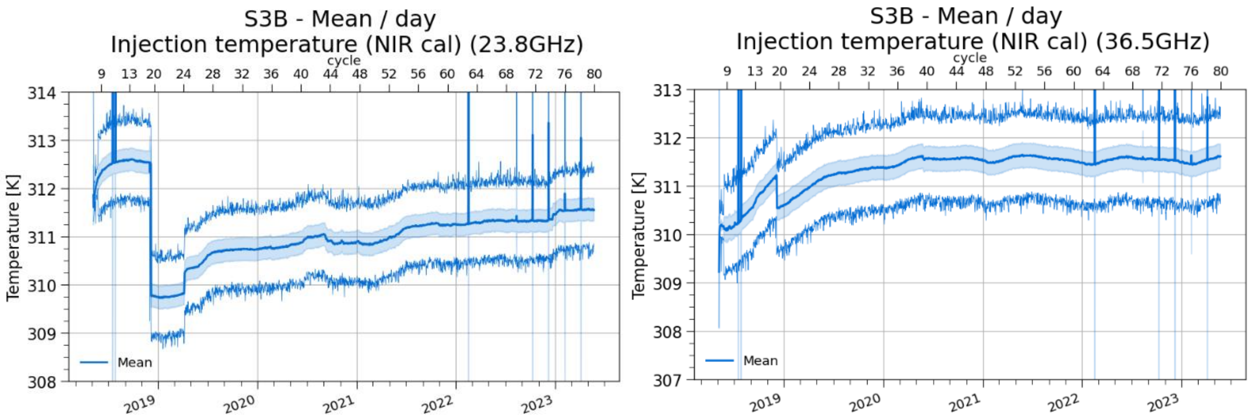

Figure 16 : Sentinel3-B Daily statistics of the noise injection temperature for channel 23.8GHz (left) and 36.5GHz (right): mean (bold line), min/max (thin line), standard deviation (shade)

5.2 Vicarious calibration

5.2.1 Coldest ocean temperatures

The first area is the ocean and more precisely the coldest temperature over ocean. Following the method proposed by Ruf [RD 1], updated by Eymar [RD 3] and implemented in [RD 7], the coldest ocean temperatures is computed by a statistic selection. Ruf has demonstrated how a statistical selection of the coldest BT over ocean allows detecting and monitoring drifts. It is also commonly used for long-term monitoring or cross-calibration [RD 4] [RD 5] [RD 6].

The Figure 17 presents the coldest ocean temperature computed following method previously described at 23.8GHz channel for Sentinel-3A/MWR and four other microwave radiometers: AltiKa/MWR, Jason3/AMR and Metop-A/AMSU-A. For AMSU-A, the two pixels of smallest incidence (closest to nadir) are averaged. The Figure 18 presents the same results for the liquid water channel of the same four instruments: 36.5GHz for Sentinel-3A, 37GHz for AltiKa , 34GHz for Jason3 and 31.4GHz for Metop-A.

Concerning the 23.8GHz channel presented on Figure 12, one can see that the temperature of the coldest ocean points is very closer to the other sun-synchroneous missions (Metop-A, SARAL/AltiKa). Jason-3 coldest temperature is almost 6K lower than the other missions because of its orbit [RD 9].

The analysis for the liquid water channel (Figure 18) is more complicated due to the different frequency used by these instruments for this channel: 36.5GHz for S3A/B, 37GHz for AltiKa, 34GHz for Jason3 and 31.4Ghz for AMSU-A. But the coldest temperatures can be used relatively one with another. For instance, one can see that the difference between AltiKa and Jason3 is about 6K which is in line with the theoretical value estimated by Brown between the channel 34 GHz of JMR and the channel 37 GHz of TMR (-5.61 K ± 0.23 K) [RD 8]. Then we can expect that Sentinel3 should be closer to AltiKa than Jason2 due to the measurement frequency. The Sentinel-3B on-the-fly NTC products show a jump in the temperatures with the update of MWR characterisation file. After the update of the MWR characterization file the 6th December, S3B presents values consistent with S3A as expected. S3B monitoring shown below represents on-the-fly data, and not the reprocessed data. Monitoring over reprocessed data would not shown the steps due to IPF configuration update, such as MWR characterisation file.

Monitoring of both channels show a small annual cycle due to the annual cycle of water vapor. This signal can be determined and removed to facilitate the comparison between mission and the assessment of the stability. Figure 19 and Figure 20 present the residuals after such processing for both channels. The residuals are small for all missions, below 0.5K in absolute value. Sentinel-3A/B are perfectly consistent with the other missions. S3B is ligthly more noisier than S3A, because the timeseries is not homogeneous and relativately short. Over the period of study, no drift is noticed for S3A or S3B.

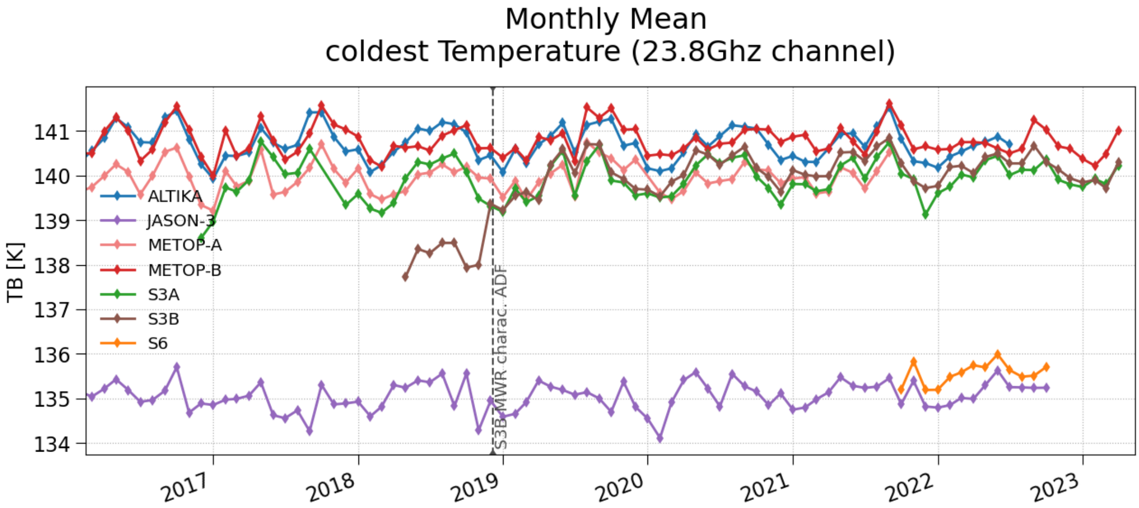

Figure 17 : Coldest temperature over ocean at 23.8GHz for S3A/B, SARAL/AltiKa, Jason2, Jason3 and Metop-A/AMSU-A

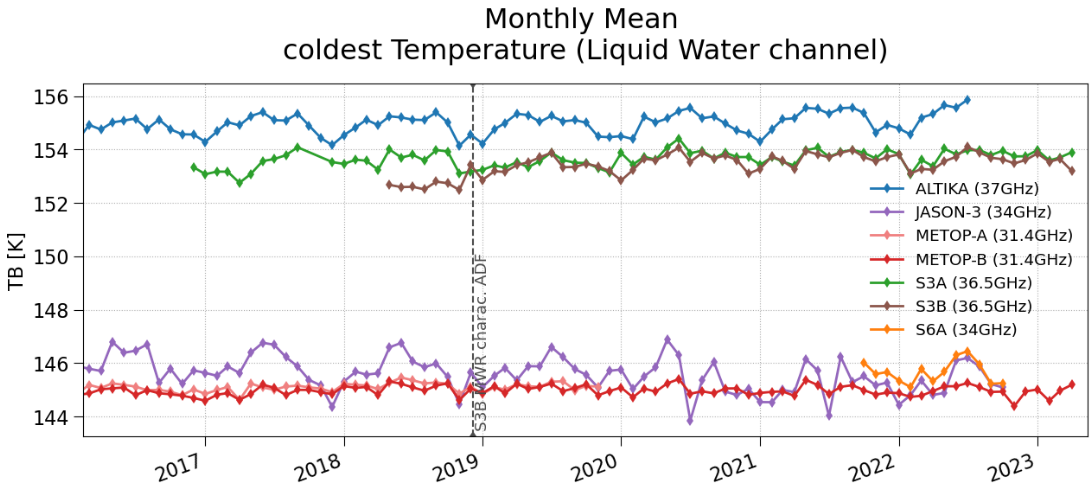

Figure 18 : Coldest temperature over ocean for the liquid water channel S3AB, SARAL/AltiKa, Jason2, Jason3 and Metop-A/AMSU-A

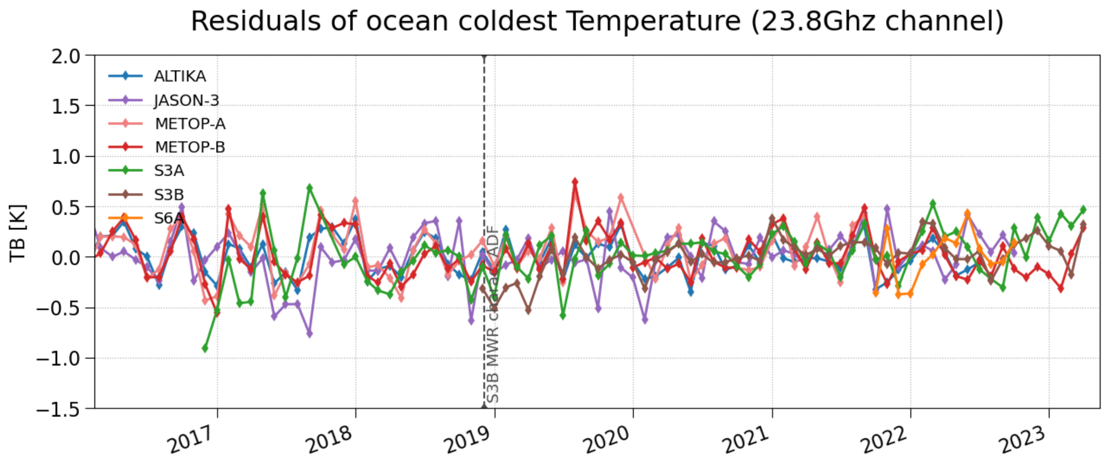

Figure 19 : Residuals after removal of yearly signal over ocean at 23.8GHz for S3A/B, SARAL/AltiKa, Jason3, S6A, and Metop-A/AMSU-A

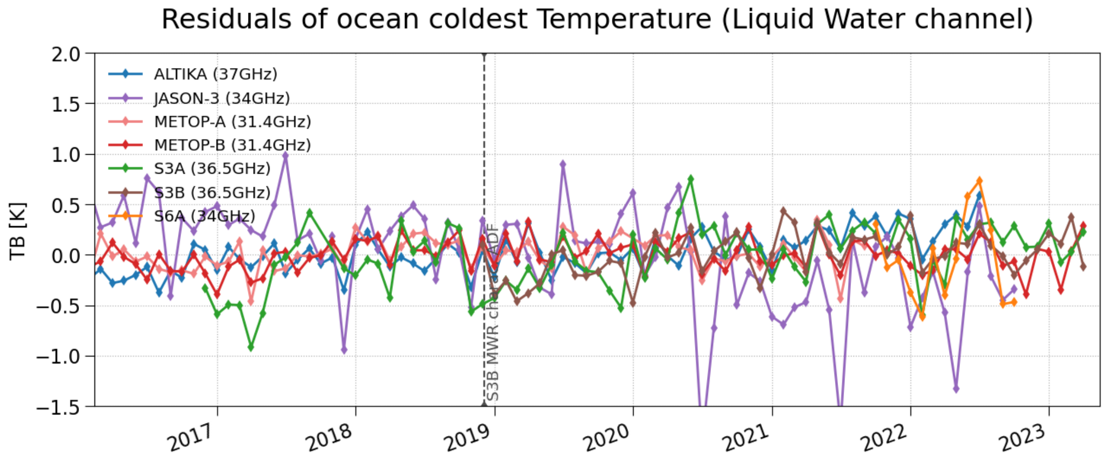

Figure 20 : Residuals after removal of yearly signal over ocean at 23.8GHz for S3A/B, SARAL/AltiKa, Jason3, S6A, and Metop-A/AMSU-A

5.2.2 Amazon forest

The second area is the Amazon forest which is the natural body the closest to a black body for microwave radiometry. Thus it is commonly used to assess the calibration of microwave radiometers [RD 2][RD 3]. The method proposed in these papers have been used as a baseline to propose a new method implemented in [RD 7]. In this new approach, a mask is derived from the evergreen forest class of GlobCover classification over Amazon. The average temperature is computed here over a period of one month for all missions.

The averaged temperature over the Amazon forest is shown on Figure 21 and Figure 22 for water vapor channel (23.8GHz) and liquid water channel respectively. These two figures show the very good consistency of S3A/B with the three other radiometers on the hottest temperatures: around 286K for the first channel, and 284K for the second channel. The mean value as well as the annual cycle is well respected. These results show the correct calibration for the hottest temperatures. At the beginning of S3B mission, no bias is observed for the hottest temperatures. After the update of the MWR characterization file the 6th December 2018, a small bias of 0.3K is introduced between S3B and S3A as expected from the commissioning phase results. S3B monitoring shown below represents on-the-fly data, and not the reprocessed data. Monitoring over reprocessed data would not shown the steps due to IPF configuration update, such as MWR characterisation file.

In autumn 2017, Metop-A starts drifting from its normal orbit to extend the mission lifetime of four years (source: https://www.eumetsat.int/science-blog/extending-working-lifetime-metop-weather-satellite). At the beginning of the mission, the Local Time of Ascending Node was 21h30. As the orbit will be drifting, the LTAN will move up to 18:00. The drift of LTAN is not constant but is accelerating with time. It did have no impact on hottest temperature selection up to end of 2019 approximately. After 2020, time of overflight shall be updated for the selection of Amazon points in order to have a sufficient number of point. In the long-term, a drift may be observable anyway if the local time of observation is not accounted for.

The annual signal can be determined and removed to facilitate the comparison between mission and the assessment of the stability. Figure 23 and Figure 24 present the residuals after such processing for both channels. El Nino event of 2016 is clearly observable with the residuals, showing an anomaly up to +1.5K The residuals are small for all missions, below 0.5K in absolute value. There are however a little large than the residuals for the coldest ocean points. The signal is noisier and more sensible to interannual variations. Sentinel-3A/B are perfectly consistent with the other missions. Over the period of study, no drift is noticed for S3A or S3B.

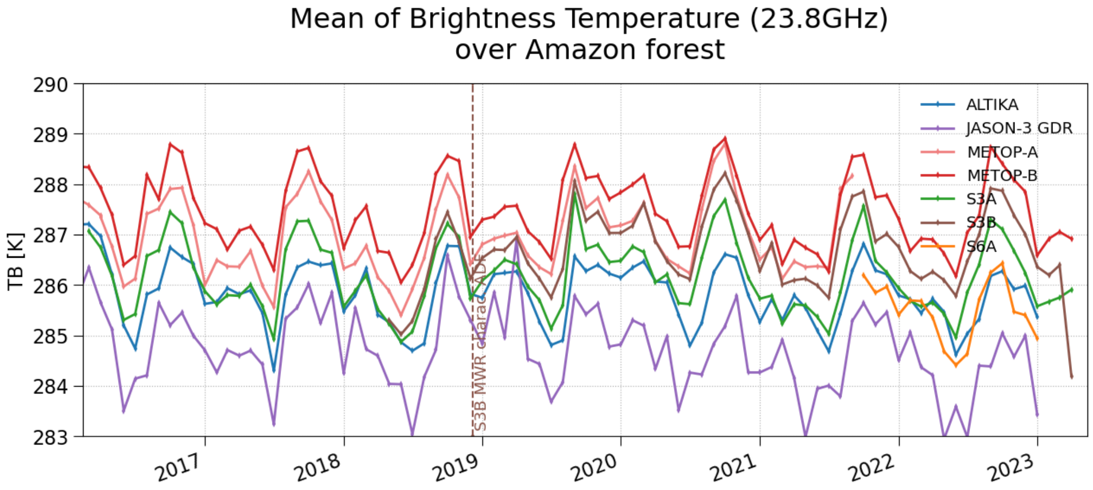

Figure 21 : Average temperature over Amazon forest at 23.8GHz channel for S3A/B, SARAL/AltiKa, Jason2, Jason3, S6A, and Metop-A/AMSU-A

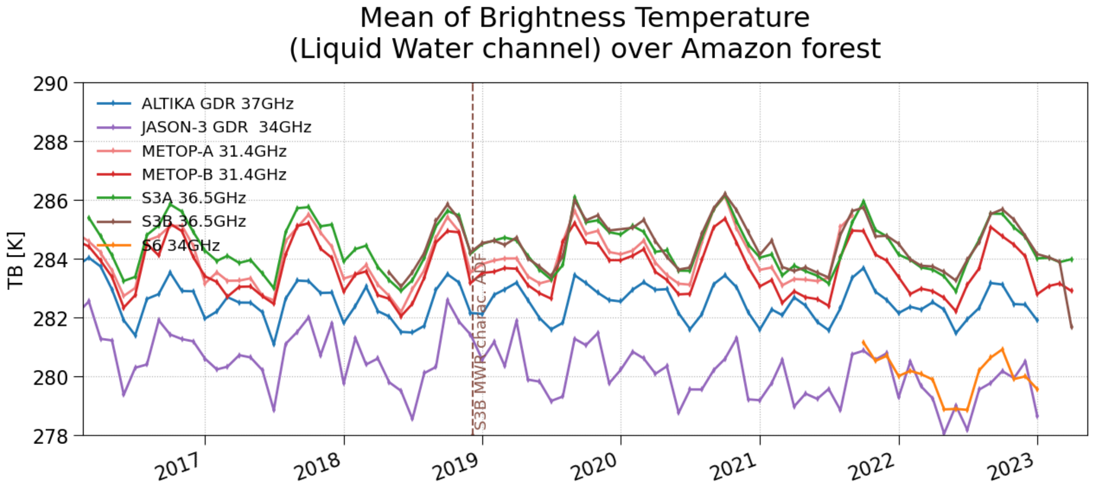

Figure 22 : Average temperature over Amazon forest at 36.5GHz channel for S3A/B, SARAL/AltiKa, Jason3, S6A, and Metop-A/AMSU-A

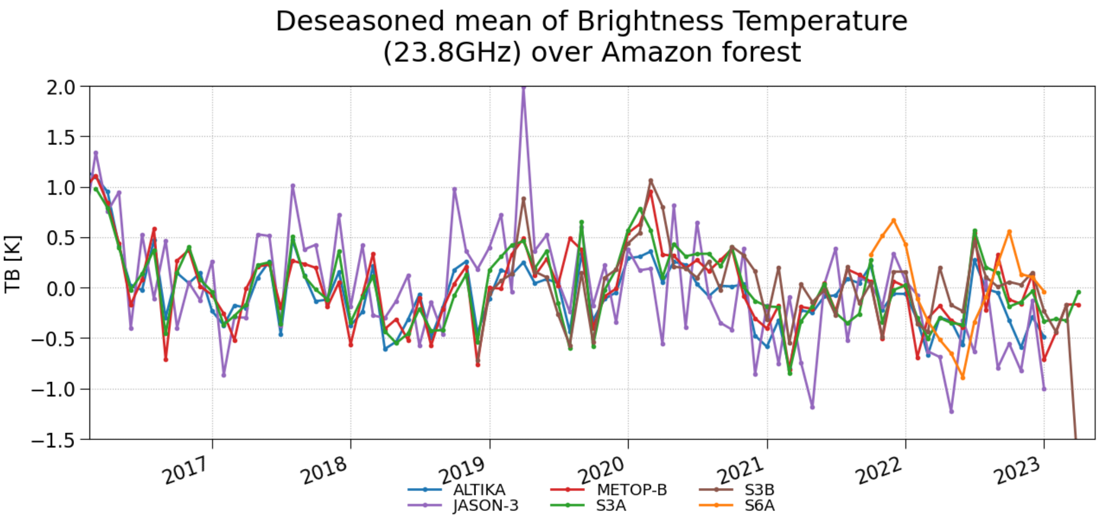

Figure 23 : Residuals after removal of yearly signal over Amazon forest at 23.8GHz channel for S3A/B, SARAL/AltiKa, Jason3, S6A, and Metop-A/AMSU-A

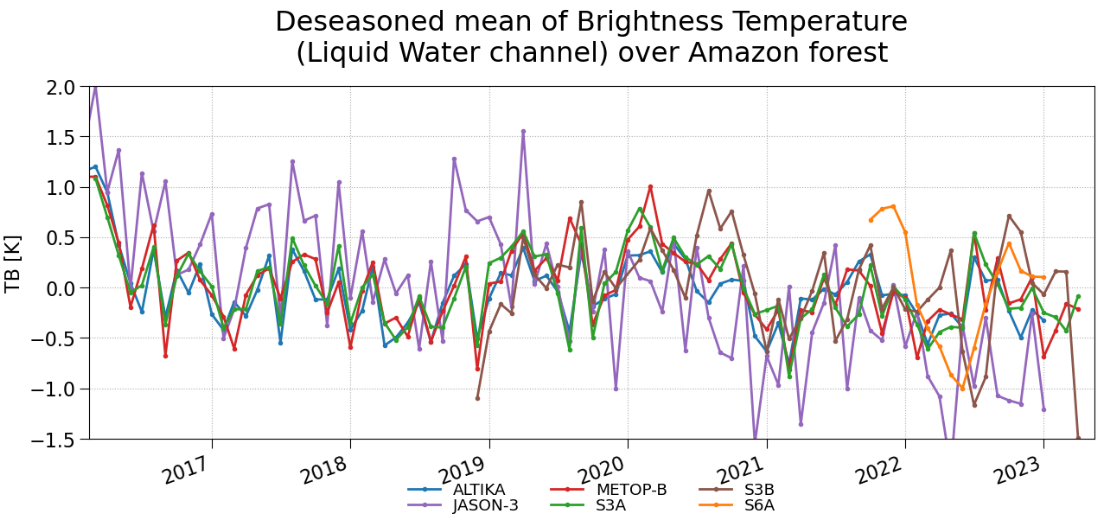

Figure 24 : Residuals after removal of yearly signal over Amazon forest at liquid water channel for S3A/B, SARAL/AltiKa, Jason3, S6A, and Metop-A/AMSU-A

6 Geophysical parameters monitoring

6.1 Monitoring of geophysical products

In this section, comparisons of difference MWR-model fields will be performed for several instruments. The selected instruments are Jason3/AMR, Sentinel-6, and SARAL/AltiKa. For a long-term monitoring perspective, GDR products are used to compute the difference with respect to model values. Model values for each field are computed using ECMWF analyses data. GDR products for each mission have their own latency due to cycle curation and mission constraints such as the cold-sky calibration for and Jason-3 missions. Indeed, AltiKa GDR is available with delay of 35 days, while for Jason3 this delay is up to 60 days.

In this section, we propose to propose to illustrate the performance of the products on specified hydrologic targets large enough to have a significant number of land-free MWR measurements. Several targets have been considered so far:

- Caspian Sea
- Baltic Sea (soon)

6.1.1 Caspian Sea

Caspian Sea is the world largest inland body of water, covering a surface of 372 000 m². It shares borders with several countries between Europe and Asia: Kazakhstan, Iran, Azerbaijan, Russia, Turkmenistan. It is overflown by several tracks of Sentinel-3A and Sentinel-3B.

6.1.1.1 Wet tropospheric correction

Figure 25 illustrates the difference MWR-ECMWF of Wet tropospheric correction (ΔWTC) for Sentinel-3A and Sentinel-3B over Caspian Sea. The map shows small scales variabilities along tracks due to the coarse spatial and temporal resolution of ECMWF correction. Note that the data periods used for S3A and S3B processing are not identical. These diagnoses will be refined more in the future reports, S3A and S3B timeseries will be completed up to the beginning of the mission.

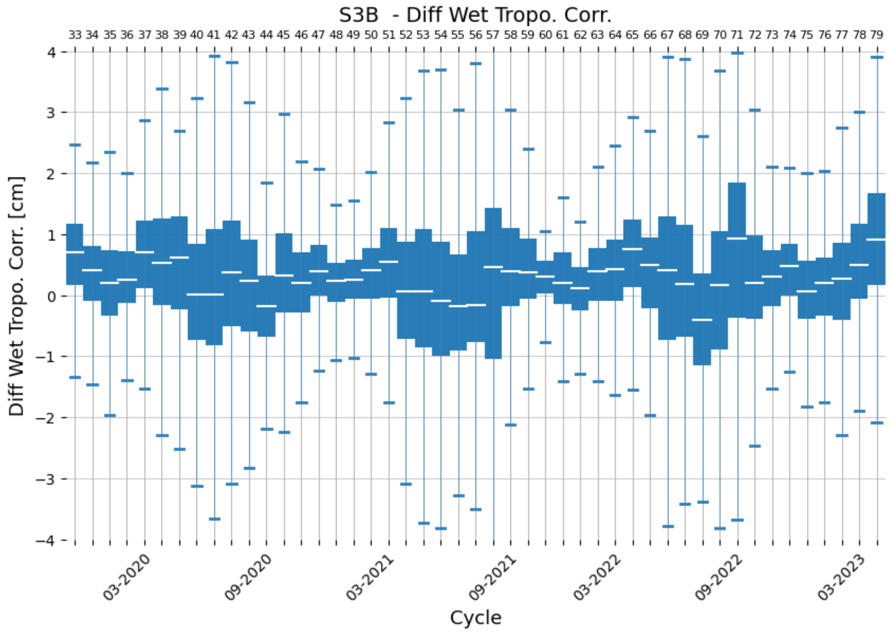

Figure 26 presents the timeseries of ΔWTC by boxplots, with the mean represented by the white line inside the box, the standard deviaton with the height of the box, and the minimum and maximum values with the whiskers. This diagnosis tracks the stability of the WTC. The timeseries seems quite stable, but standard deviation and minimum/maximum values show some seasonal evolution, with larger values during summer and smaller values during winter. Filtering of data must be assessed further to check of these variations are due to spurious data not filtered out or to a geophysical signal.

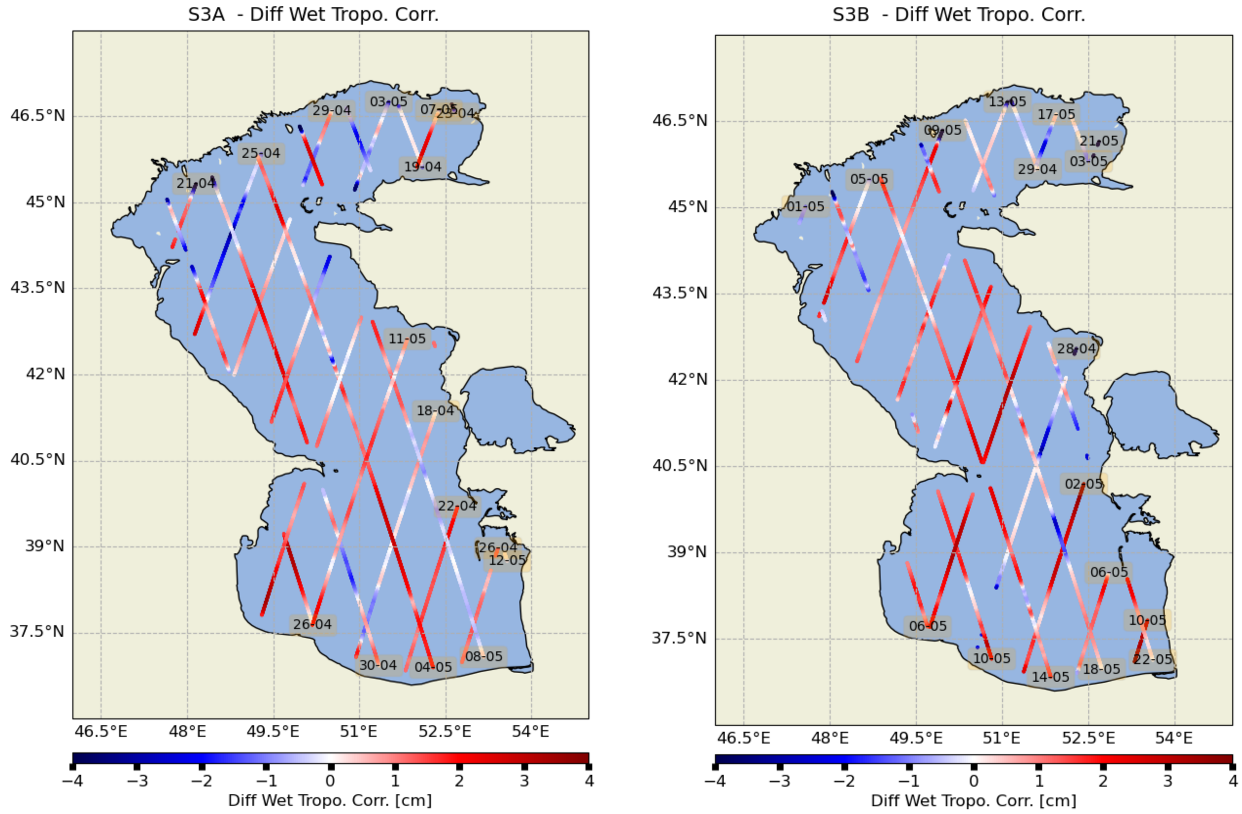

Figure 25: Difference MWR-ECMWF of WTC (SAR) on Caspian Sea for Sentinel-3A and Sentinel-3B

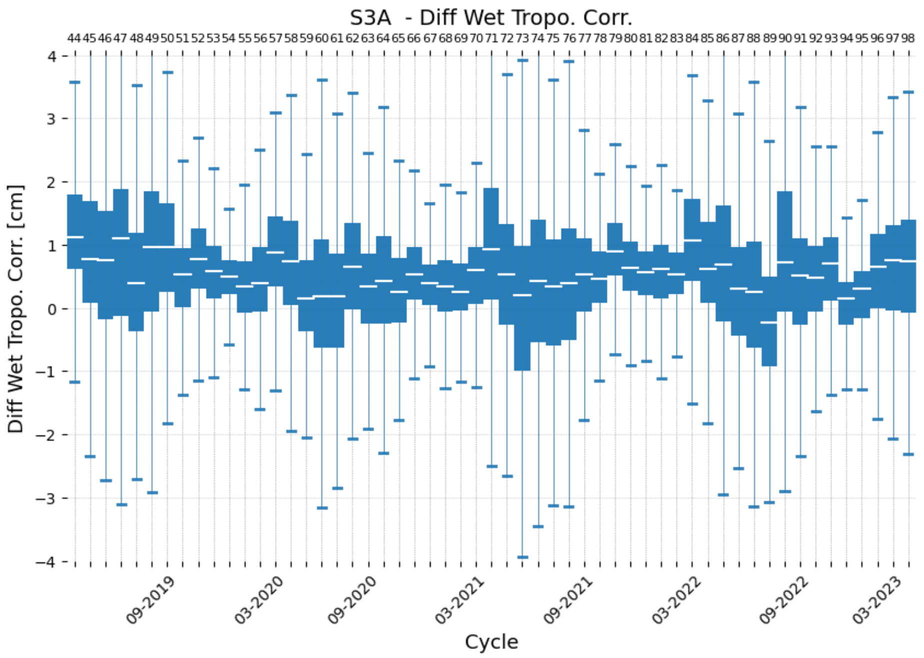

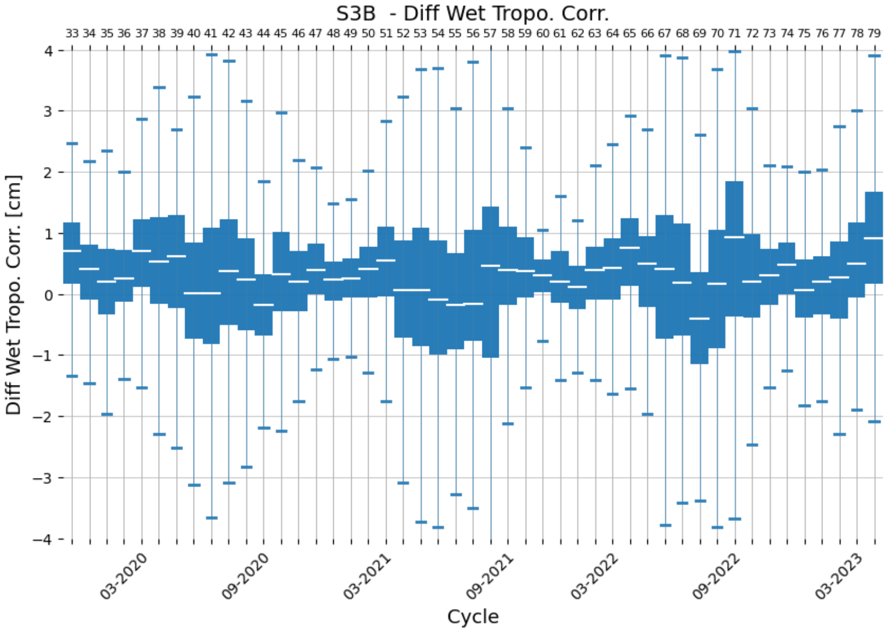

Figure 26: Timeseries of difference MWR-ECMWF of WTC (SAR) for Sentinel-3A (top) and Sentinel-3B (bottom)

6.1.1.2 Atmospheric attenuation

Figure 27 illustrates the difference MWR-ECMWF of Atmospheric attenuation of Sigma0 (ΔATM_ATT) for Sentinel-3A and Sentinel-3B over Caspian Sea. The map shows small scales variabilities along tracks due to the coarse spatial and temporal resolution of ECMWF correction. Differences are large in the presence of clouds.

Figure 28 presents the timeseries of ΔATM_ATT by boxplots, with the mean represented by the white line inside the box, the standard deviaton with the height of the box, and the minimum and maximum values with the whiskers. This diagnosis tracks the stability of the Atmospheric attenuation. The timeseries seems quite stable. Filtering of data must be assessed further to check if the variations observed in winter 2020 (cycle 65/66) are due to spurious data not filtered out or to a geophysical signal.

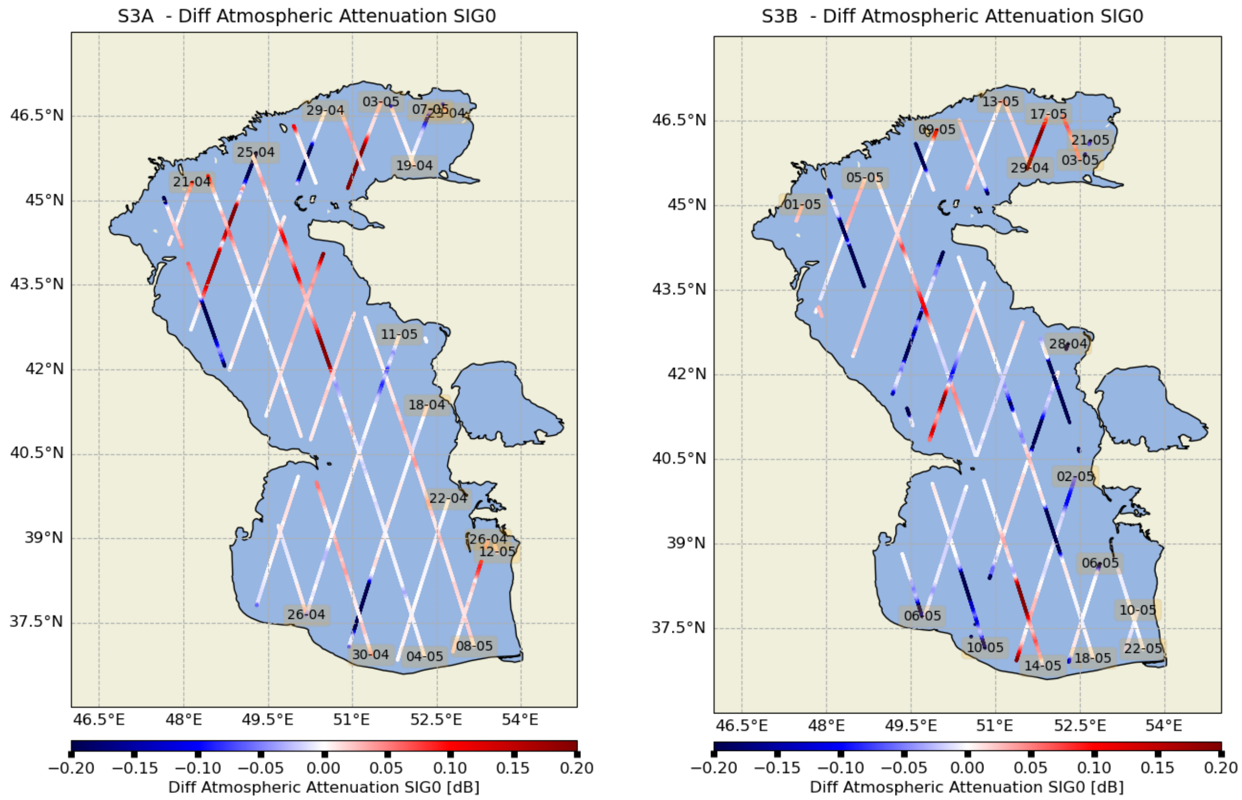

Figure 27: Difference MWR-ECMWF of Atmospheric attenuation of Sigma0 (SAR) on Caspian Sea for Sentinel-3A and Sentinel-3B

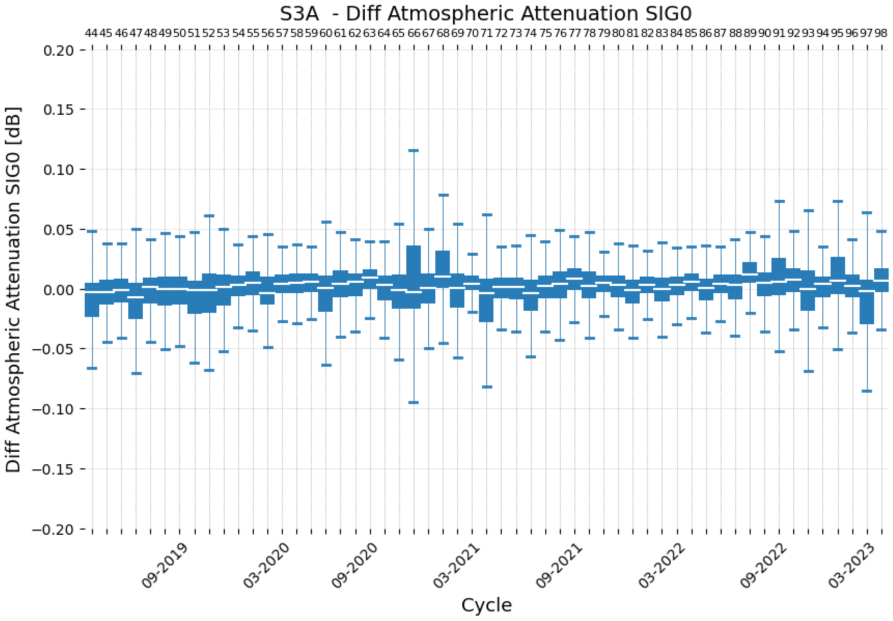

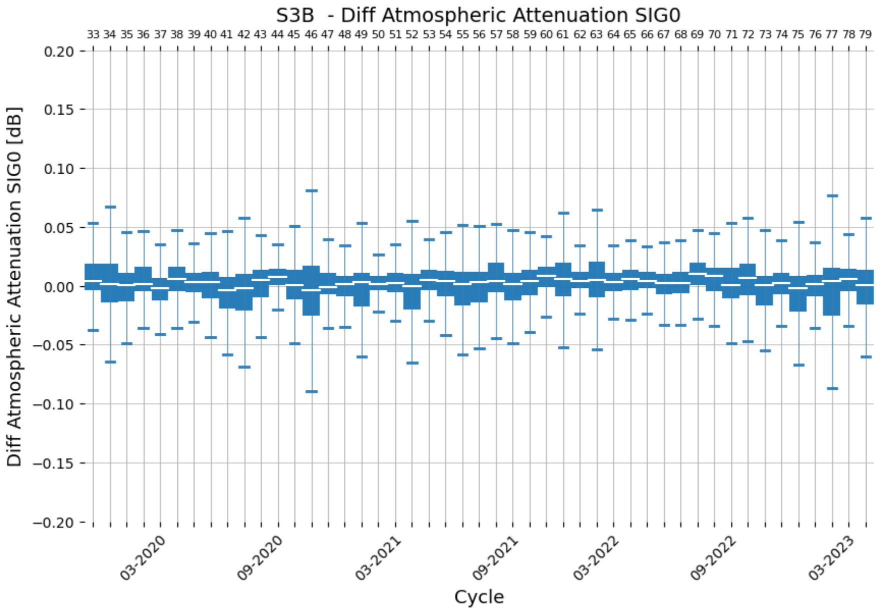

Figure 28: Timeseries of difference MWR-ECMWF of Atmospheric attenuation of Sigma0 (SAR) for Sentinel-3A (top) and Sentinel-3B (bottom)

6.1.1.3 Vapor water content

Figure 29 illustrates the difference MWR-ECMWF of Water vapor (ΔWV) for Sentinel-3A and Sentinel-3B over Caspian Sea. The map shows small scales variabilities along tracks due to the coarse spatial and temporal resolution of ECMWF correction. Differences are large in the presence of clouds.

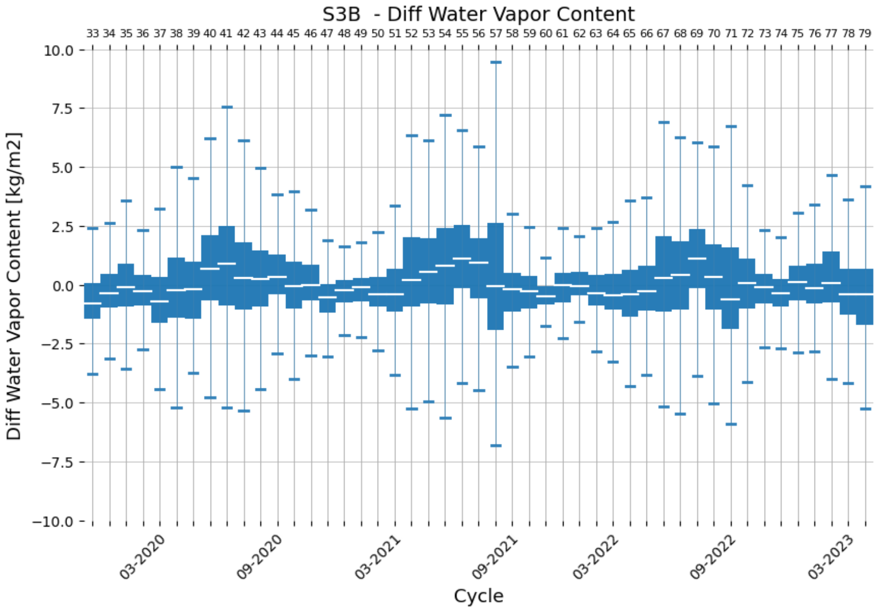

Figure 30 presents the timeseries of ΔWV by boxplots, with the mean represented by the white line inside the box, the standard deviaton with the height of the box, and the minimum and maximum values with the whiskers. This diagnosis tracks the stability of the Atmospheric attenuation. The timeseries seems quite stable, but standard deviation shows some seasonal evolution, with larger values during summer and smaller values during winter. Data filtering must be assessed further to check of these variations are due to spurious data not filtered out or to a geophysical signal. As expected, the behavior observed for the water vapor content is very similar to the WTC timeseries (

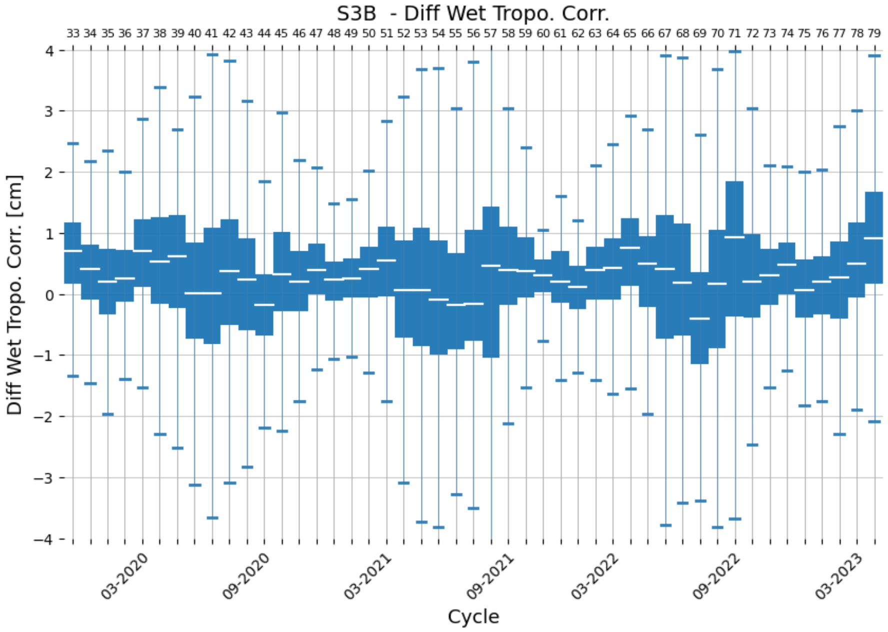

Figure 26).

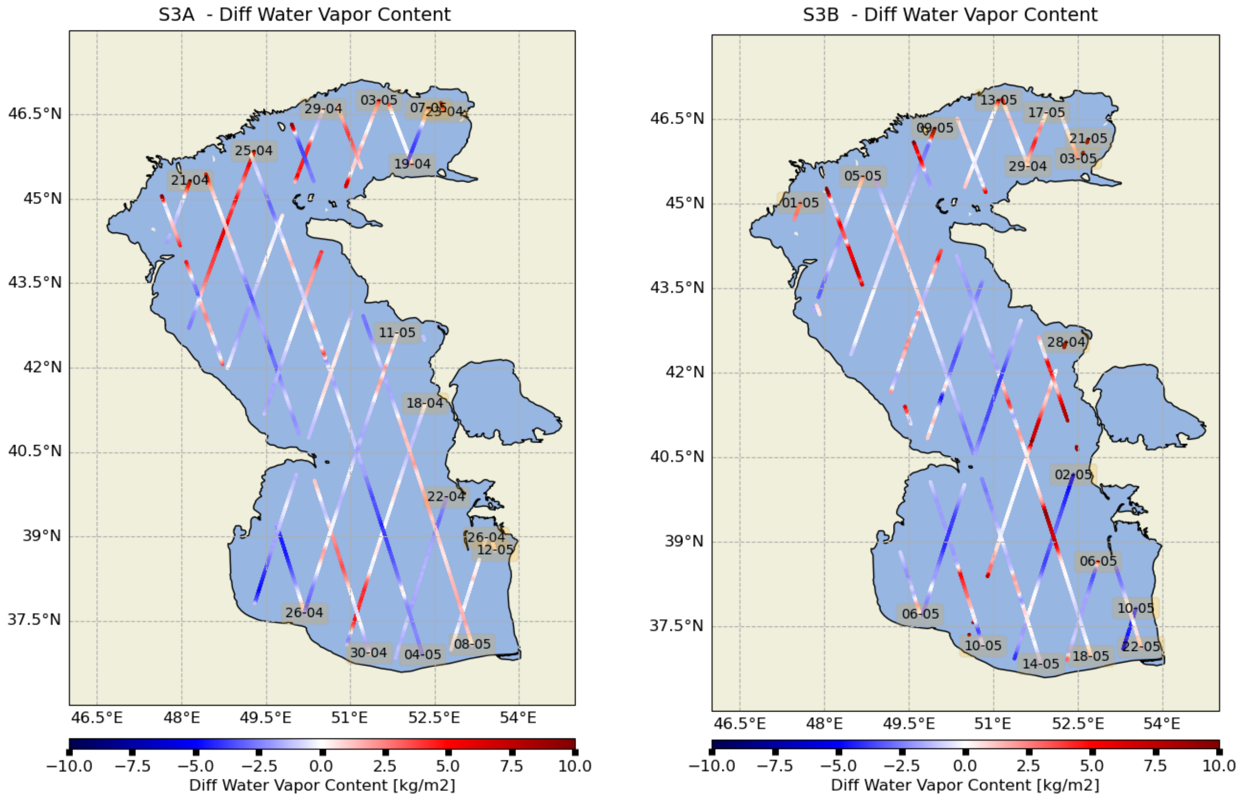

Figure 29: Difference MWR-ECMWF of Water vapor on Caspian Sea for Sentinel-3A and Sentinel-3B

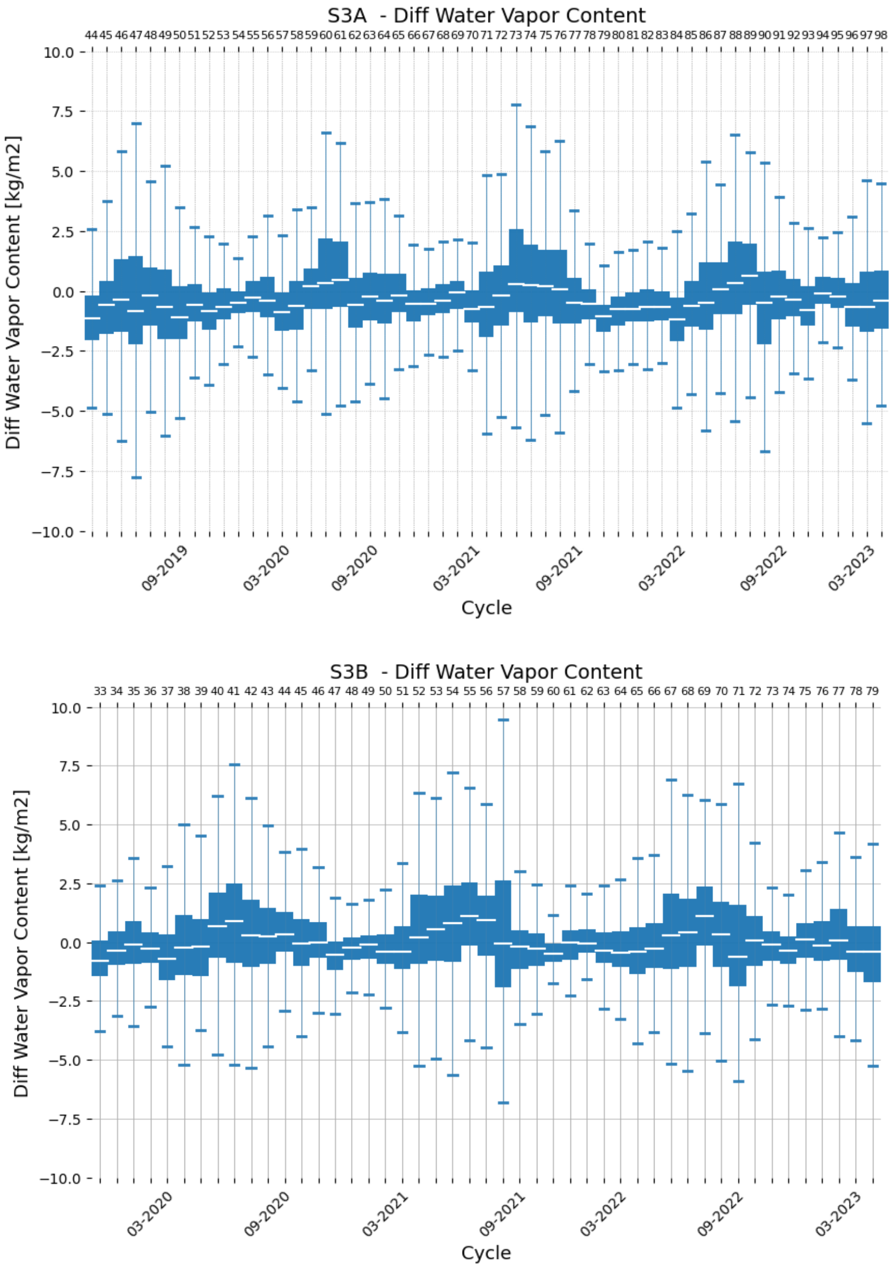

Figure 30: Timeseries of difference MWR-ECMWF of Water vapor for Sentinel-3A (top) and Sentinel-3B (bottom)

6.1.1.4 Cloud liquid water content

Figure 31 illustrates the difference MWR-ECMWF of Cloud liquid water content (ΔWC) for Sentinel-3A and Sentinel-3B over Caspian Sea. The map shows small scales variabilities along tracks due to the coarse spatial and temporal resolution of ECMWF correction. Differences are large in the presence of clouds.

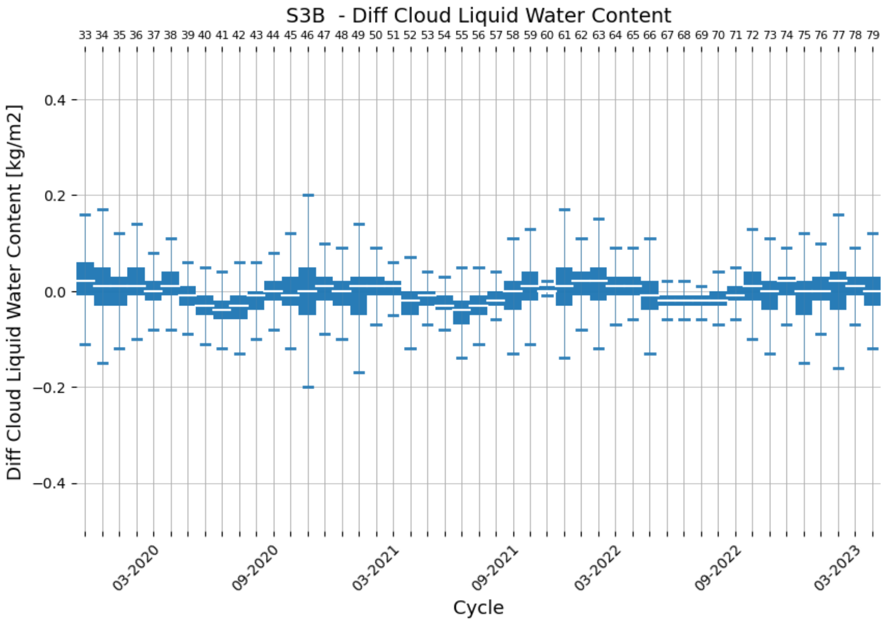

Figure 32 presents the timeseries of ΔWC by boxplots, with the mean represented by the white line inside the box, the standard deviaton with the height of the box, and the minimum and maximum values with the whiskers. This diagnosis tracks the stability of the Cloud liquid water content. The timeseries seems quite stable, but standard deviation shows some seasonal evolution, with larger values during summer and smaller values during winter. Filtering of data must be assessed further to check of these variations are due to spurious data not filtered out or to a geophysical signal.

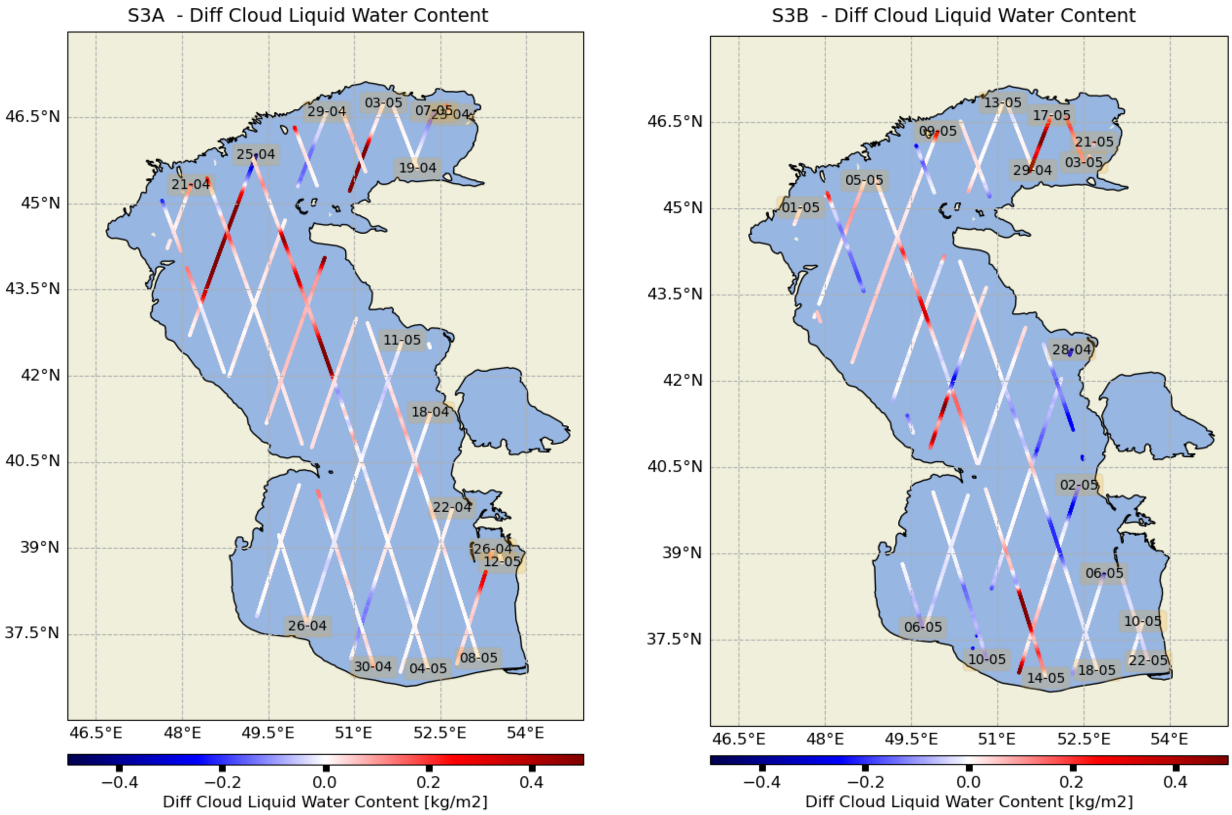

Figure 31: Difference MWR-ECMWF of Cloud liquid water content on Caspian Sea for Sentinel-3A and Sentinel-3B

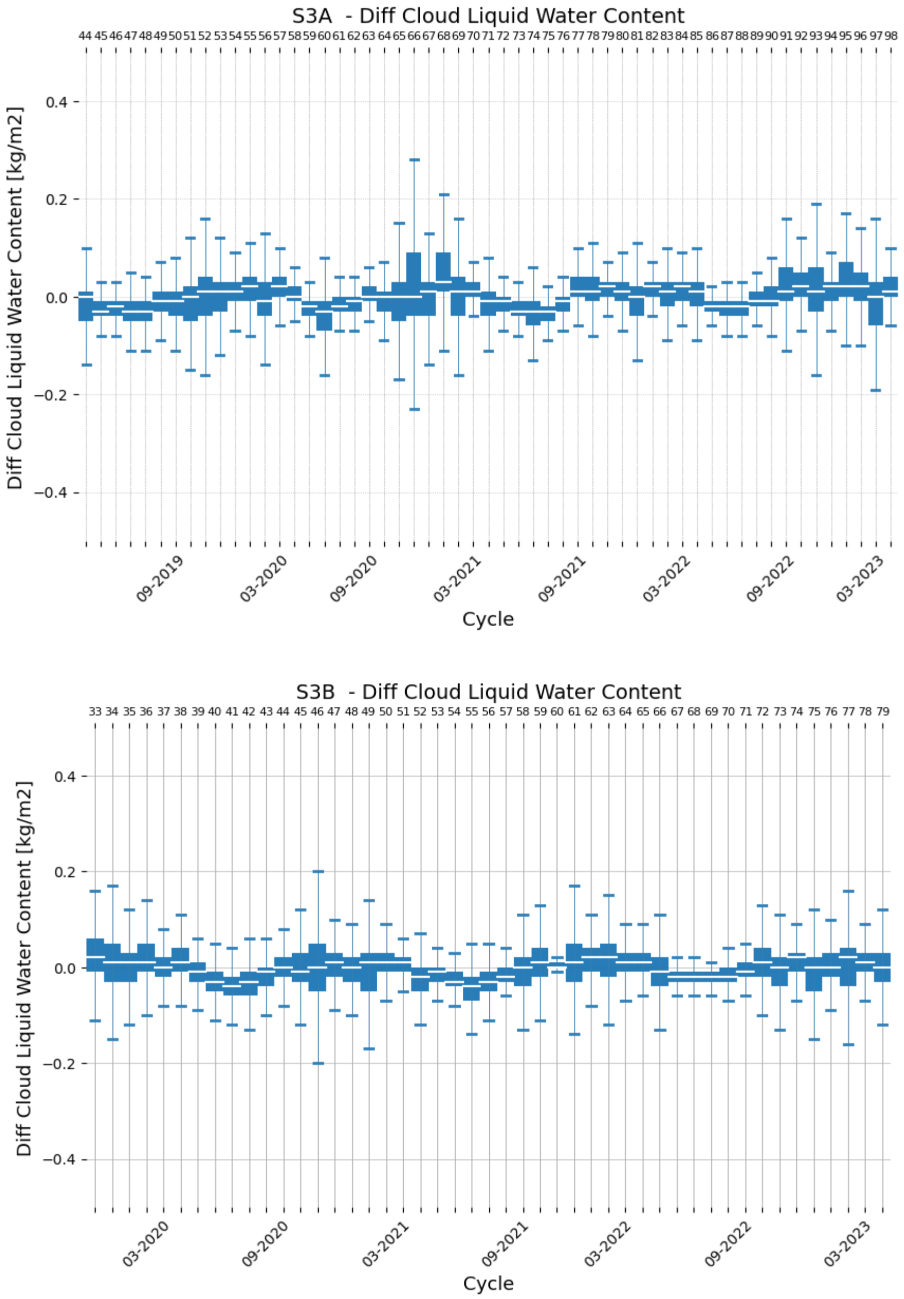

Figure 32: Timeseries of difference MWR-ECMWF of Cloud liquid water content for Sentinel-3A (top) and Sentinel-3B (bottom)

6.2 Comparison to in-situ measurements

6.2.1 Comparison to radiosonde observations

Several networks exist as provider of radiosonde data. For the time being, we are using radiosonde observations provided by IGRA network (Integrated Global Radiosonde Archive). This archive [http://www.ncdc.noaa.gov/oa/climate/igra/] gathers around 1500 stations from 1963 up to now. A quality control is applied on each station but there is no bias correction of the raw measurements.

This network provides measurements for open ocean islands, coastal and land stations. On this study, we applied the method proposed by S. Brown during the JMR on-orbit calibration (S. Brown, C. Ruf, S. Keihm, and A. Kitiyakara, “Jason Microwave Radiometer Performance and On-Orbit Calibration,” Mar.

Geod., vol. 27, no. February 2015, pp. 199–220, 2004.). The first step is to select a subset of open ocean stations. Over this batch of open ocean station, we will work with stations close enough in space and time of S3A track (500km;9h) and a sufficient number of coincident measurements for the analysis. Figure 33 shows the coverage of all stations (blue and red points), red points are the stations selected for the analysis of S3A data.

The wet tropospheric correction derived from profile’s humidity and temperature measurements are compared to the MWR correction at the closest approach point with no land contamination. To avoid land contamination, a minimum distance from shoreline of 25km is required.

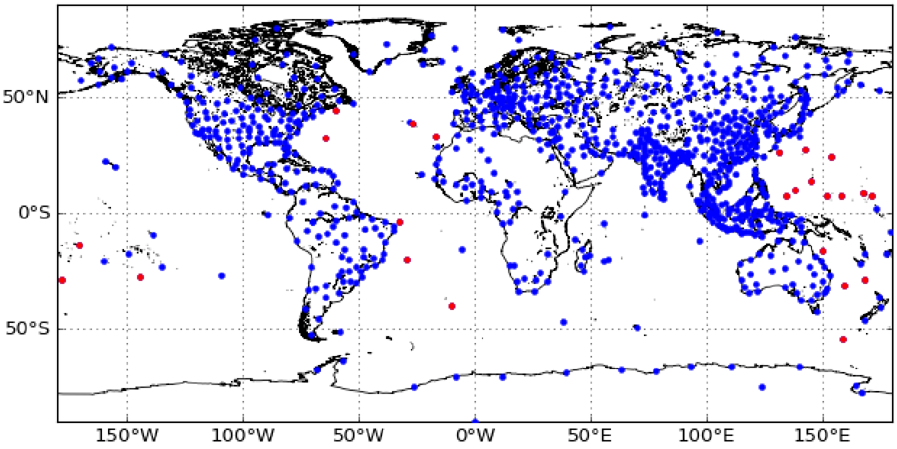

Figure 33: IGRA archive coverage (blue+red). Red points are the stations selected for comparison to S3A wet tropospheric correction.

Diagnosis to be updated for Land Sentinel-3 products.

6.2.2 Comparison to GPS observations

For the comparison to GPS measurements, we started by using the Suominet database (https://www.suominet.ucar.edu). The project is a university-based GPS network developed for atmospheric research presented in this paper:

Ware, R.H., D.W. Fulker, S.A. Stein, D.N. Anderson, S.K. Avery, R.D. Clark, K.K. Droegemeier, J.P. Kuettner, J.B. Minster, and S. Sorooshian, 2000: SuomiNet: A Real-Time National GPS Network for Atmospheric Research and Education. Bull. Amer. Meteor. Soc., 81, 677–694, https://doi.org/10.1175/1520-0477(2000)081<0677:SARNGN>2.3.CO;2

The network exploits the ability of ground-based GPS receivers to perform hourly measurements of the lower and upper atmospheres. Estimations of the wet and dry path delay can be performed from these GPS measurements. Measurements are provided every half-hour.

For this analysis, a selection of stations is performed with the following criteria:

- Providing data along the full period 2016-2022
- Providing valid value of the wet delay
- Close to S3A ground track
- Position of the station far from ice: some stations can be rounded by ice seasonally, thus MWR will be contaminated and the retrieved wet tropospheric correction will not be accurate.

Using the criteria mentioned above, we selected 19 stations indicated by the red points in Figure 34.

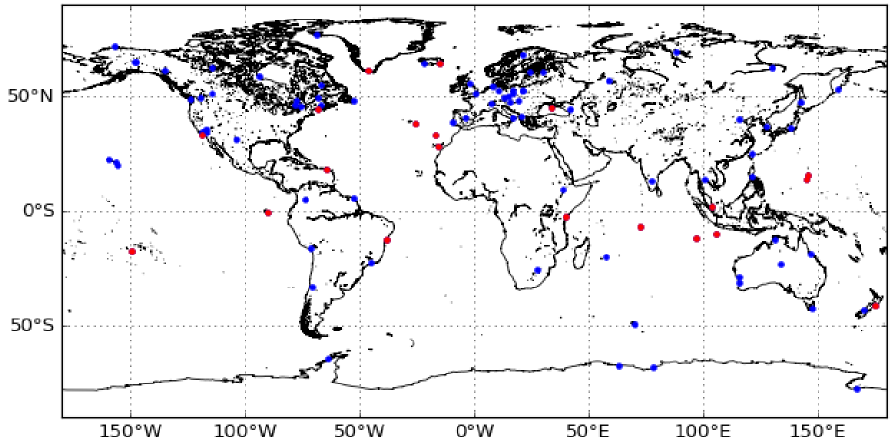

Figure 34: Map of stations of Suominet network: all (blue), selected for comparison to S3 MWR (red)

The selection in space is the same than for the radiosonde. The selection in time is easier in the context of the comparison with GPS as it provides measurements every 30 minutes. It means that if the ground track of S3A or S3B is close to a GPS station, the minimum time difference between MWR and GPS will be 30 minutes at maximum. To avoid land contamination, a minimum distance from shoreline of 25km is required.

Appendix A - Useful links

The Product Format Specification applicable to the MWR Level 1 products assessed in this report is available in Sentinel Online, version 2.13:
https://sentinel.esa.int/documents/247904/0/Sentinel-3-Product-Data-Format-Specification-Level-1-products/2b7c773b-44ca-447e-9b86-f7ebd231261c

Appendix B - References

RD 1 C. Ruf, 2000: Detection of Calibration Drifts in spaceborne Microwave Radiometers using a Vicarious cold reference, IEEE Trans. Geosci. Remote Sens., 38, 44-52

RD 2 S. Brown, C. Ruf, 2005: Determination of an Amazon Hot Reference Target for the on-orbit calibration of Microwave radiometers, Journal of Atmos. Ocean. Techno., 22, 1340-1352

RD 3 L. Eymard, E. Obligis, N. Tran, F. Karbou, M. Dedieu, 2005: Long term stability of ERS-2 and TOPEX microwave radiometer in-flight calibration, IEEE Trans. Geosci. Remote Sens., 43, 1144-1158

RD 4 C. Ruf, 2002: Characterization and correction of a drift in calibration of the TOPEX microwave radiometer, IEEE Trans. Geosci. Remote Sens., 40, 509-511

RD 5 R. Scharoo, J. Lillibridge, W. Smith, 2004: Cross-calibration and long-term monitoring of the microwave radiometers of ERS, TOPEX, GFO, Jason and Envisat, Marine Geodesy, 27, 279-297

RD 6 R. Kroodsma, D. McKague, C. Ruf, 2012: Inter-Calibration of Microwave Radiometers Using the Vicarious Cold Calibration Double Difference Method, Applied Earth Obs. and Remote Sensing, 5, 1939-1404

RD 7 Estimation des dérives et des incertitudes associées pour les radiomètres micro-ondes. Revue des méthodes existantes, SALP-NT-MM-EE-22288,

RD 8 Brown, S., C. Ruf, S. Keihm, and A. Kitiyakara, “Jason Microwave Radiometer Performance and On-Orbit Calibration,” Mar. Geod., vol. 27, no. 1–2, pp. 199–220, 2004.